Chapter 3
Laser Cooled Atomic Physics

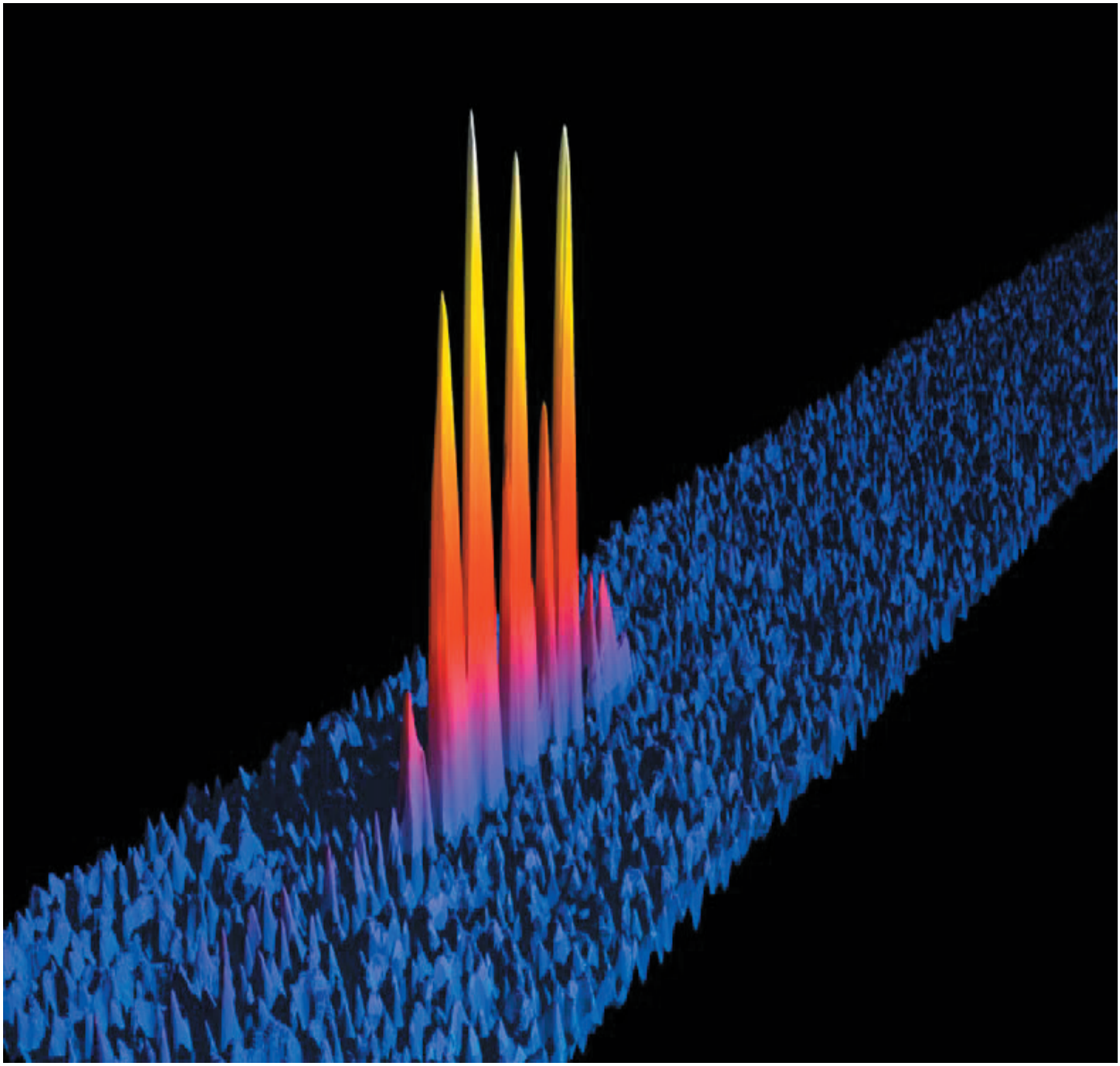


Fermion Superfluidity
Kevin Strecker
Andrew Truscott
Guthrie Partridge
Ying-Cheng Chen
RICE
UNIVERSITY

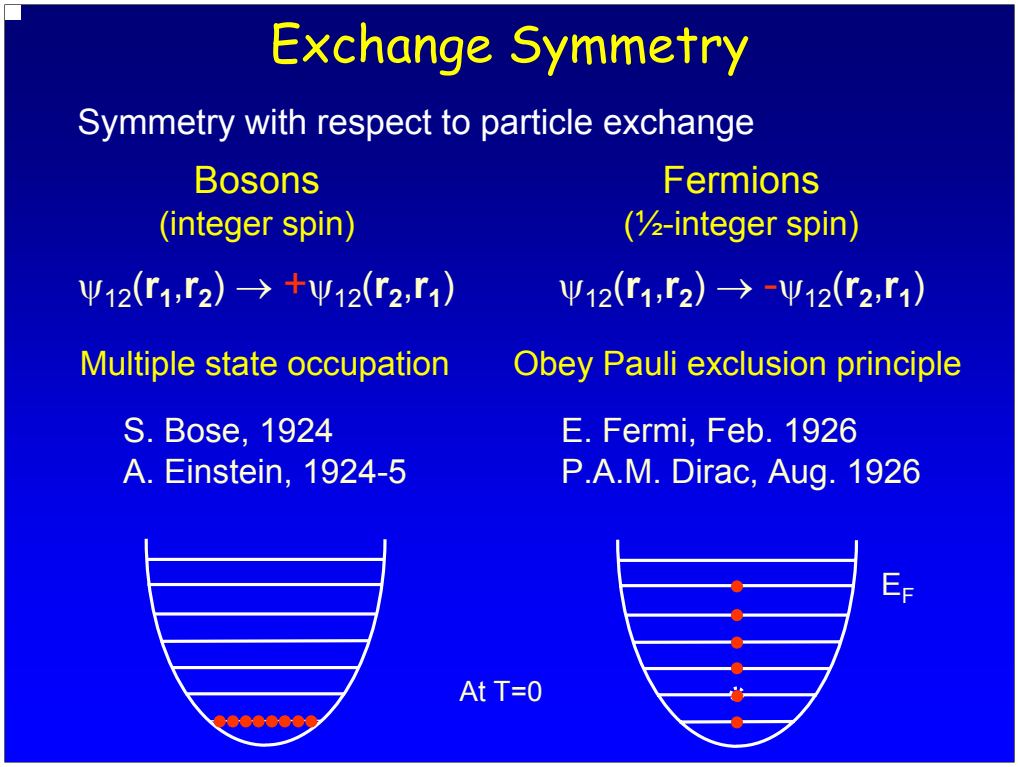

Fermions and bosons differ in respect to particle exchange. This difference leads to a completely different hierarchy of quantum state occupation at low temperatures.

Ultracold Fermi Gases – The Next Frontier?

- Building blocks of matter
- Connections to condensed matter
  - Superconductivity (high-T_c?)
  - Pseudo-gap
  - Lattices
  - Luttinger liquid, spin-charge separation, …

Fermions are the building blocks of matter. Consequently, many of the important paradigms of condensed matter physics can be realized with cold atomic gas that obey Fermi statistics. However, because the densities in cold atom experiments are many orders of magnitudes less than those in condensed matter, these systems are much simpler theoretically.

BCS/Pairing Transition

- Cooper pairing
  - Superconductivity
  - Superfluidity ^{3}He
  - Dilute gas?
- For *s*-wave pairing, $T_c \cong T_F \exp(-1/k_F|a|)$ (BCS)
- For ^{6}Li, a = -1100 Å $\Rightarrow$ T_c = 30 nK @ 10^{12} cm^{-3}
  - Stoof *et al.*, PRL **76**, 10 (1996)
- Interactions variable for quantum gases
  - current theories break down for strong coupling:

$k_F|a| > 1$ or $n|a|^3 > 1$

Weak coupling - BCS

Strong coupling - BEC of molecules?

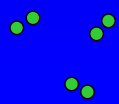

Cooper pairing is the mechanism underlying both superconductivity in certain solids, as well as superfluidity in liquid helium-3. BCS theory predicts that the transition temperature to the superfluid state depends exponentially on the scattering length a. Henk Stoof and I proposed that lithium-6 would be a good candidate for creating a Fermi superfluid in ultracold gases. However, the current theories of superconductivity and superfluidity break down for strong interactions, necessitating the development of new theory. This is currently underway at a number of institutions. In this regime, the Cooper pairs resemble loosely bound diatomic molecules.

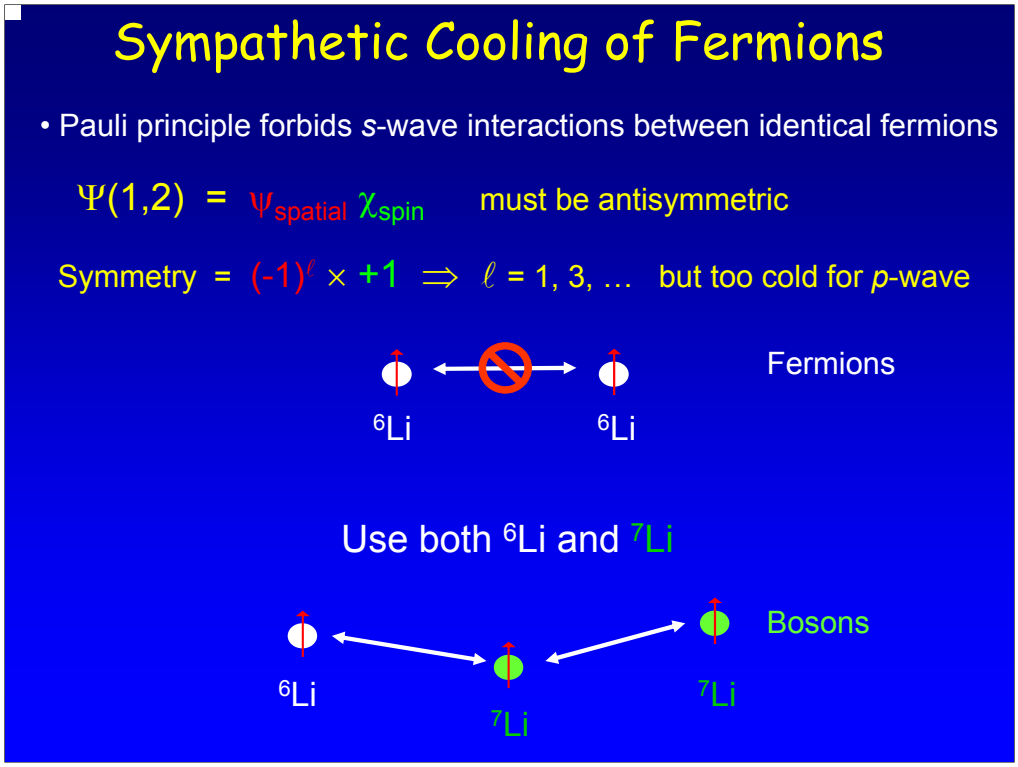

Spin-polarized fermions are forbidden to interact via *s*-wave interactions by their exchange symmetry requirement. Since other partial waves are "frozen out" by the low temperatures, a spin-polarized Fermi gas is essentially ideal. This prevents evaporative cooling by the usual direct method employed successfully to cool bosons. We use a "sympathetic" technique, where actively evaporated lithium-7 atoms (bosons) cool the lithium-6, the fermions, by thermal contact.

Quantum Degenerate Fermions

- JILA: ^{40}K, two spin states
- Rice, Paris: ^{6}Li, symp. with ^{7}Li
- Duke: ^{6}Li, two spin states in optical trap
- Florence: ^{40}K, symp. with ^{87}Rb
- MIT: ^{6}Li, symp. with ^{23}Na

A number of groups have undertaken ultracold fermion research and have adopted several different strategies for cooling the atoms.

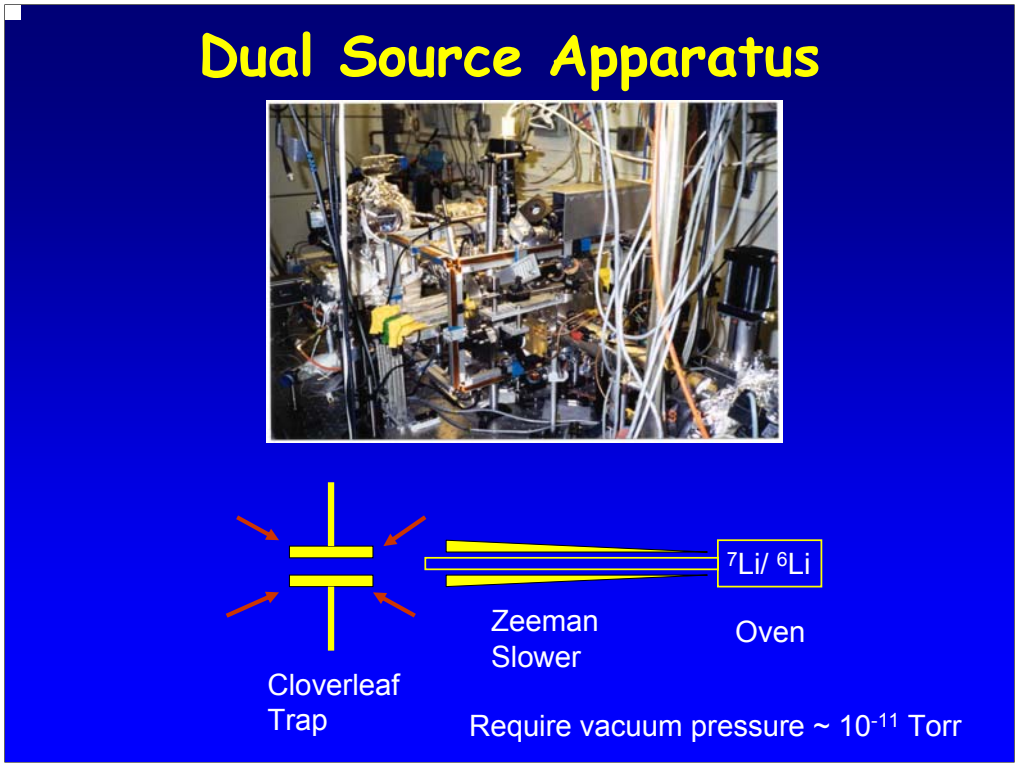

The apparatus consists of an atomic beam source, a Zeeman slower and a cloverleaf-type magnetic trap.

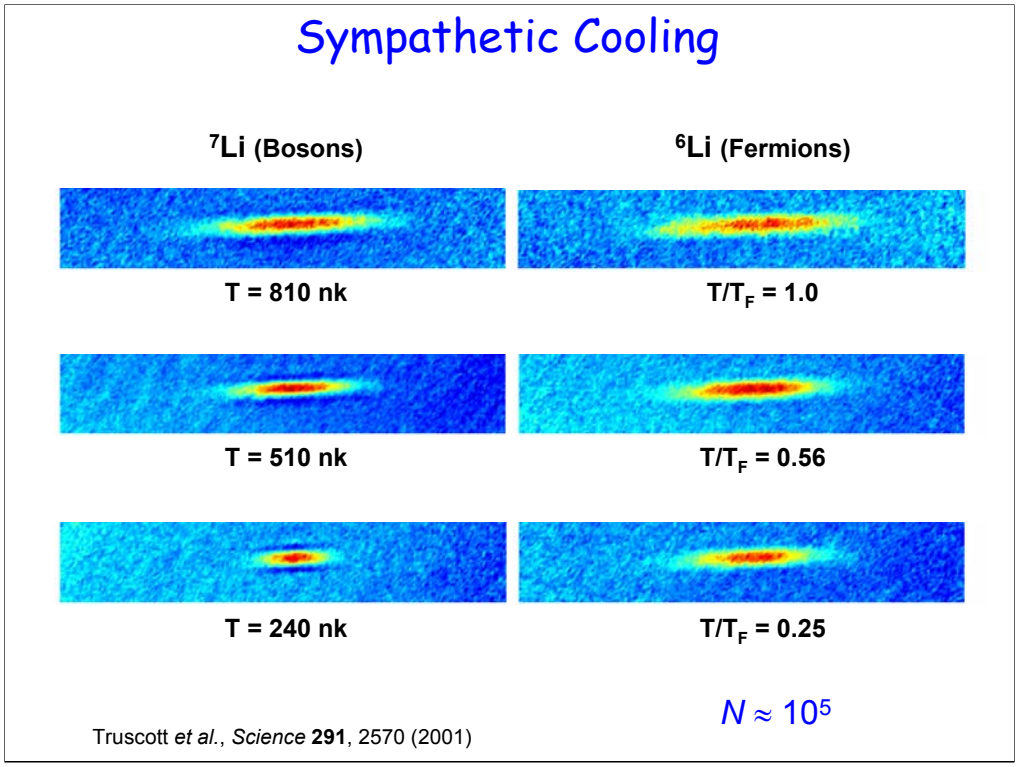

We succeeded a couple of years ago to cool the Bose/Fermi mixture of lithium isotopes to quantum degeneracy. The size and shape of the Bose cloud changes significantly with temperature as can be seen in the images on the left side. However, the fermions obey the Pauli principle which causes them to have a residual energy and pressure at zero temperature. This Fermi pressure is the same physical mechanism responsible for stabilizing white dwarf and neutron stars.

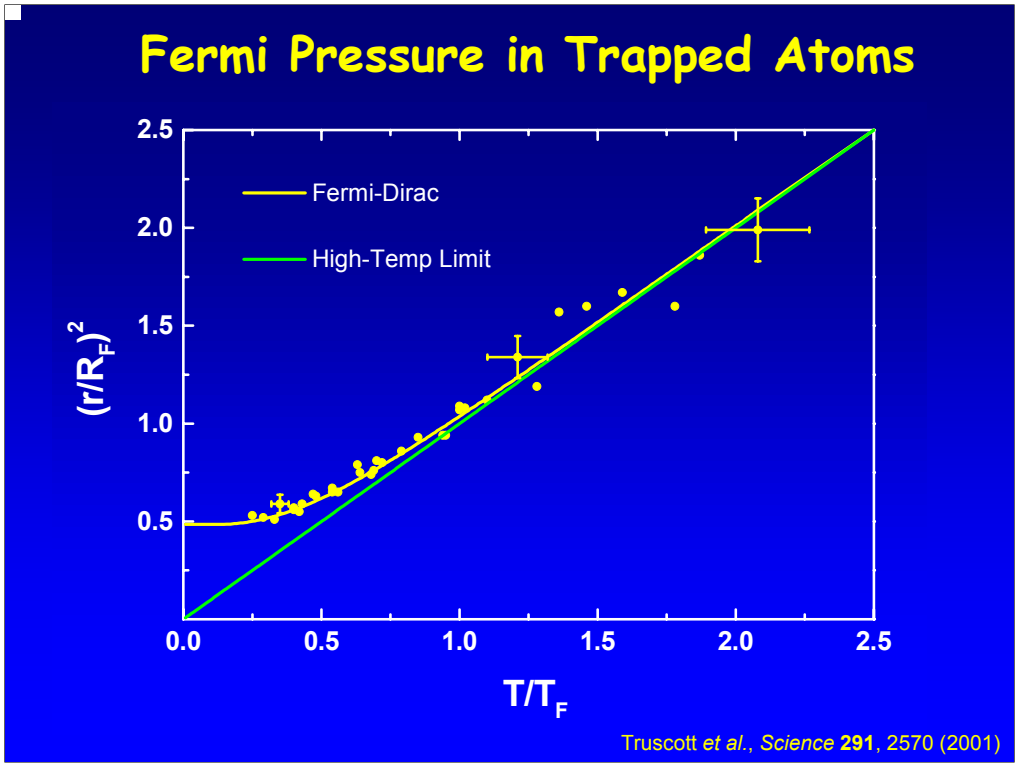

This figure shows the axial size of the fermion cloud as a function of temperature. The effect of Fermi pressure is observed at the lowest temperatures.

Limit of Sympathetic Cooling With Bosons

- Want $C_B > C_F$
- But $C_B = 11\, N_c k_B$
  and
  $C_F = \pi^2 N_F k_B (T/T_F)$
- $\Rightarrow$ $T/T_F > 0.3$

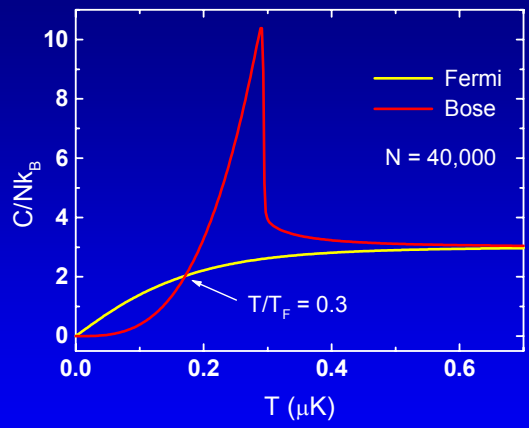

- Deeper cooling obtained by evaporation of fermions *and* bosons

Dual Evaporation

Sympathetic cooling is no longer effective when the heat capacity of the refrigerant, the bosons, falls below that of the fermions. This happens when the temperature T goes below 0.3 T_F. This limit is consistent with our minimum observed temperature of 0.25 T_F. Further cooling can be accomplished by evaporating both the fermions and bosons, a process of dual evaporation.

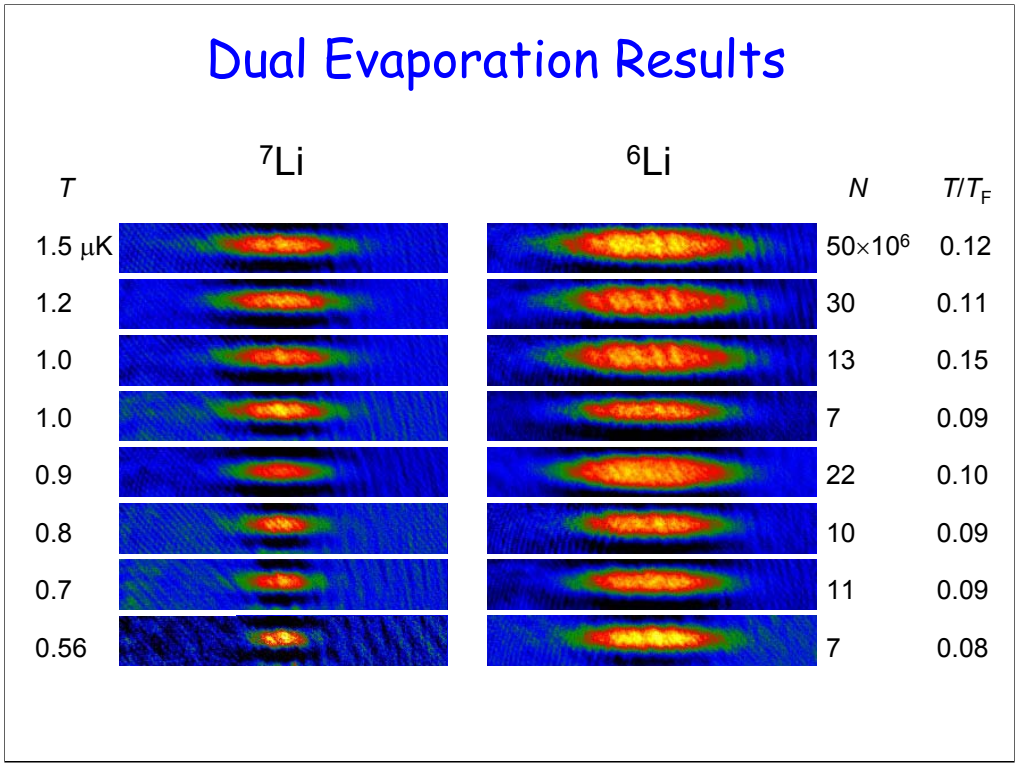

These images demonstrate the large improvement made possible by dual evaporation. We have increased the number of fermions by a factor of 100 while simultaneously lowering the minimum temperature by a factor of 3.

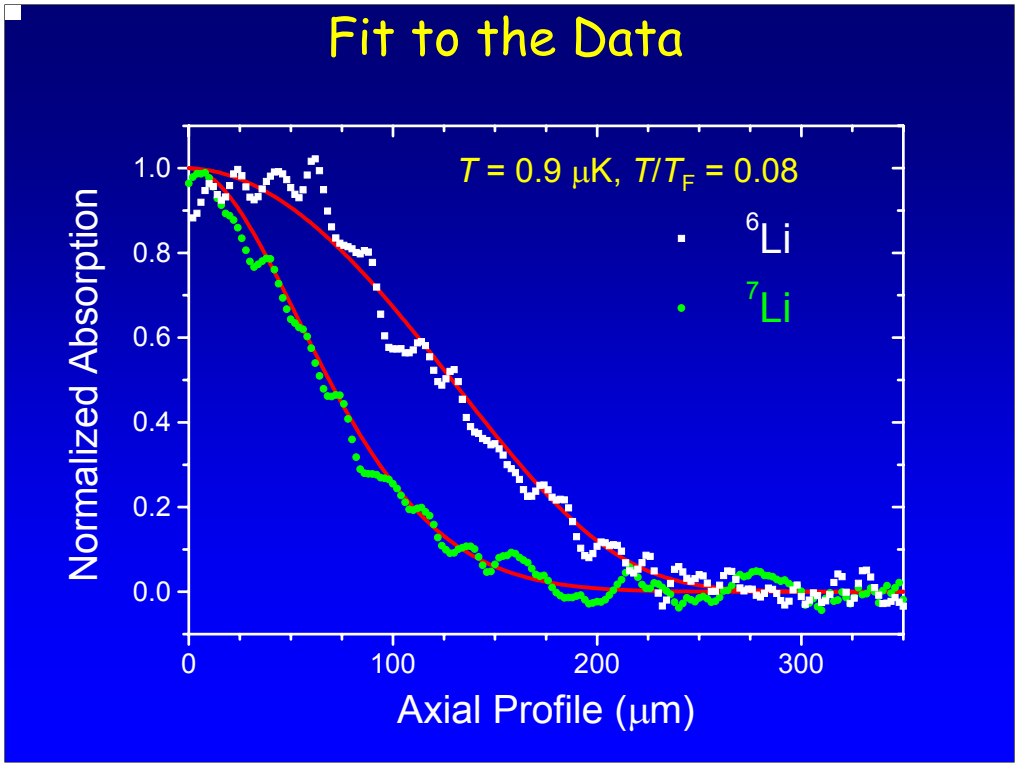

These are profiles of the density distributions for both bosons and fermions. The isotopes are in thermal equilibrium.

Cooper Pairing in ^{6}Li

S-wave pairing symmetry forbidden between identical atoms

⇒ Create *incoherent* mixture of two states

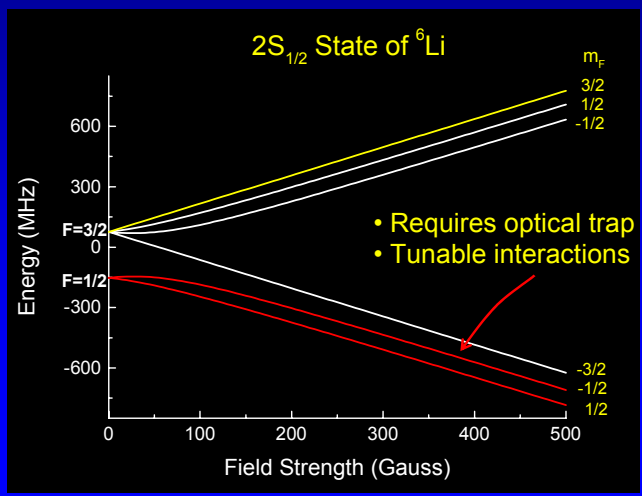

Stoof *et al.*, PRL **76**, 10 (1996)

Cooper pairing requires a large, attractive interaction. Because of the Fermi symmetry, a two-spin state incoherent mixture is needed. The lowest two Zeeman sub-levels exhibit a Feshbach resonance, that enables tunability of the interaction strength and sign, as shown in the next slide.

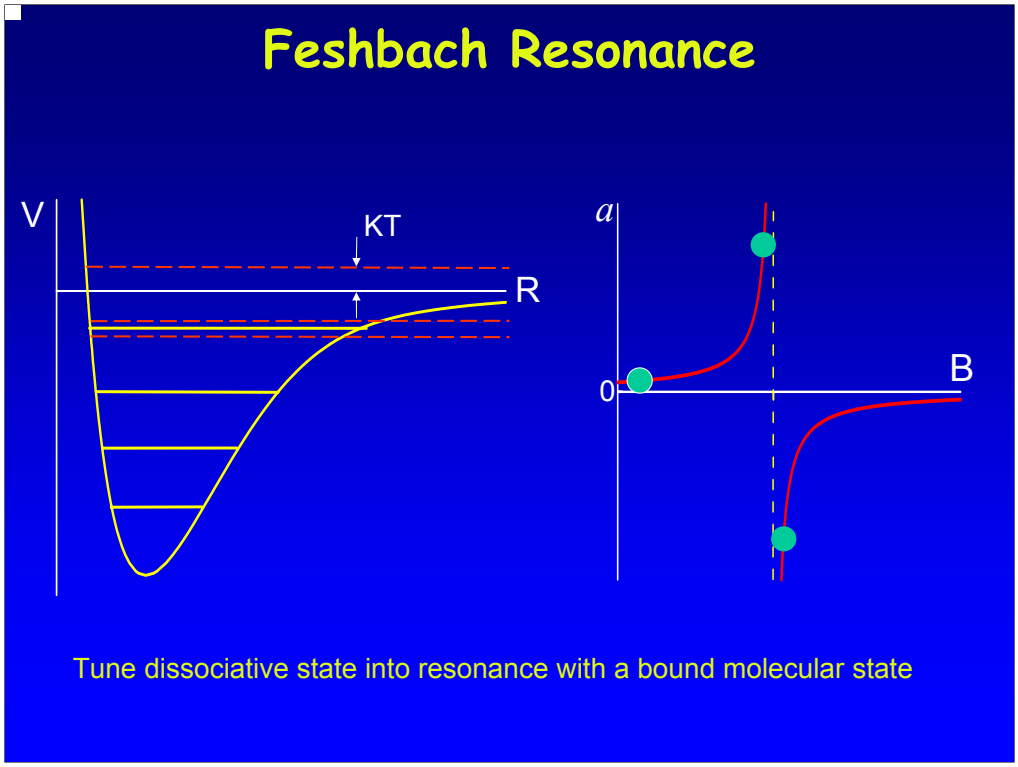

A Feshbach resonance is a magnetically tuned collisional resonance in which an open channel of two colliding free atoms is tuned near a molecular bound state. The scattering length is large and positive when the molecular state is bound, while it becomes large and negative when the molecule is unbound.

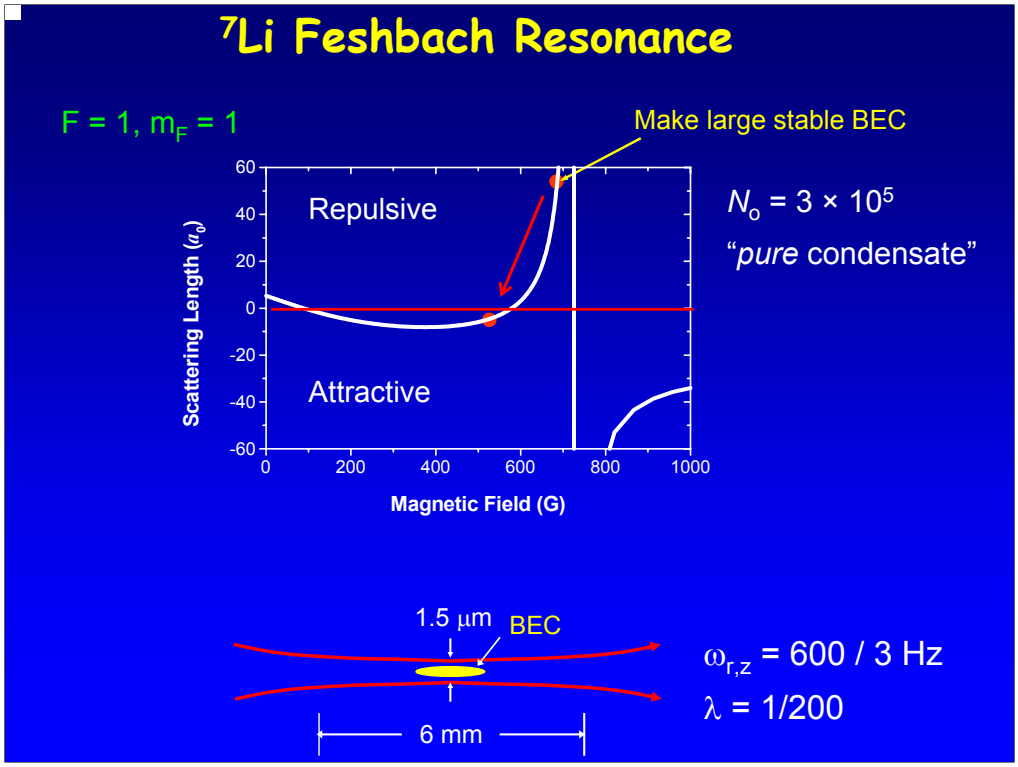

This is an example of a Feshbach resonance in the boson, lithium-7. We trapped the atoms in an optical trap and formed a Bose condensate by tuning to a field where the scattering length is positive. The field is then reduced to where the interactions are weakly attractive. If the confinement is effectively one-dimensional the condensate will form matter wave solitons.

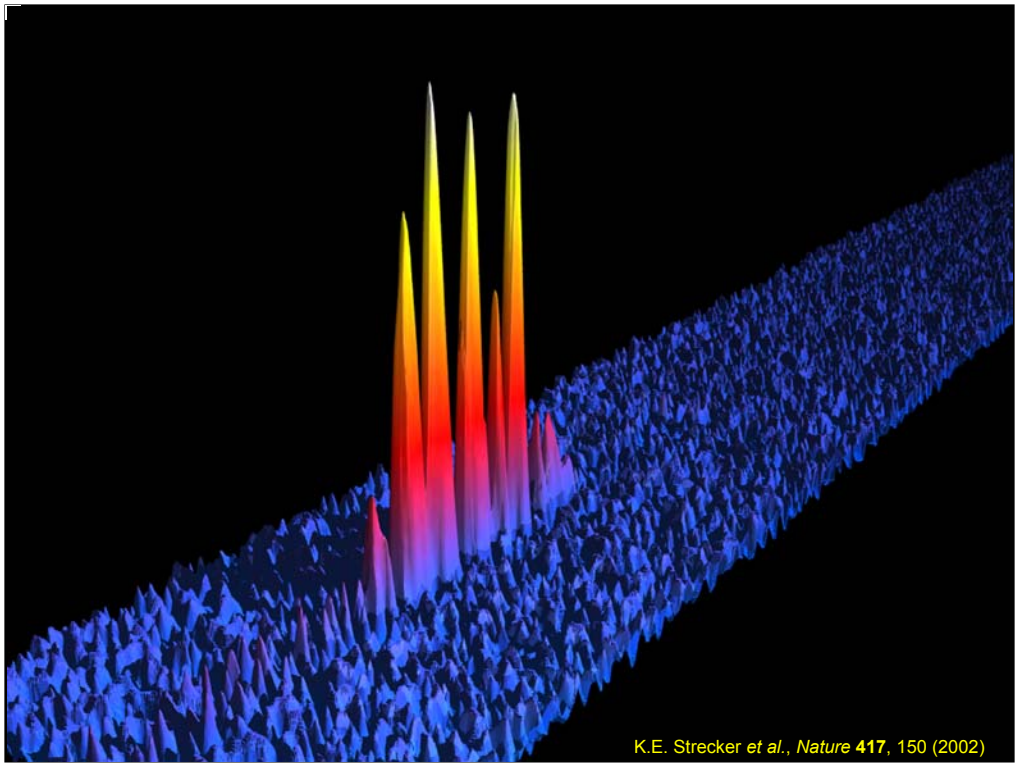

This is an image of the resulting solitons. Each peak is Bose-Einstein condensate in which wave-packet dispersion is balanced by attractive interactions.

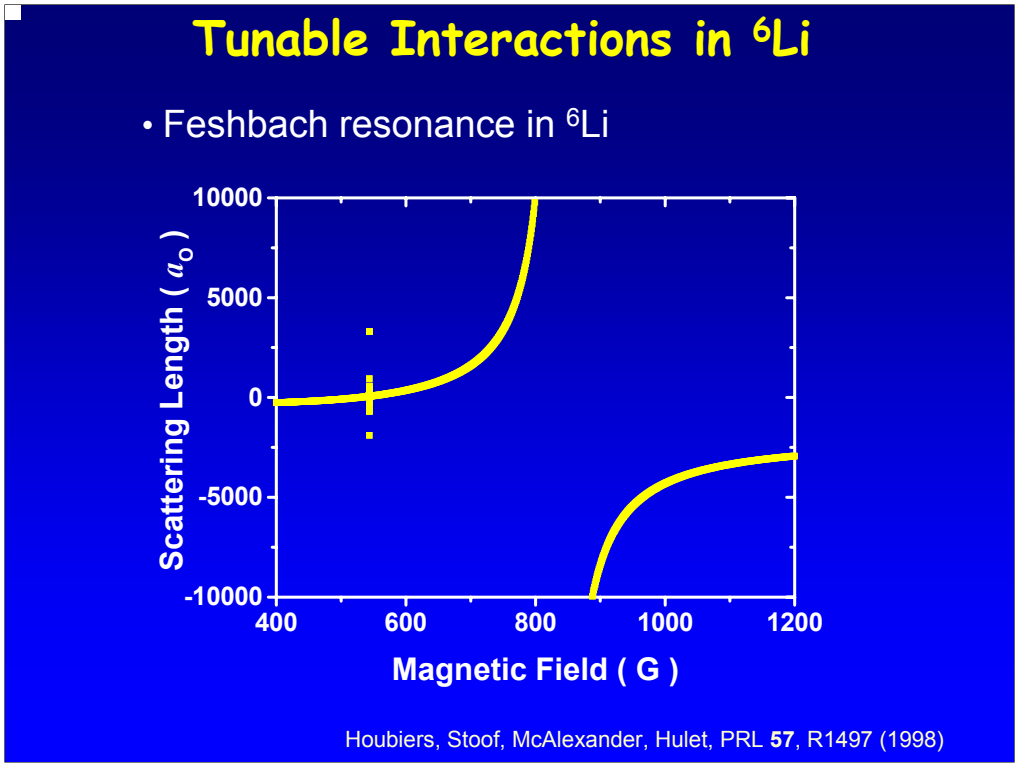

This is the calculated Feshbach resonance for lithium-6.

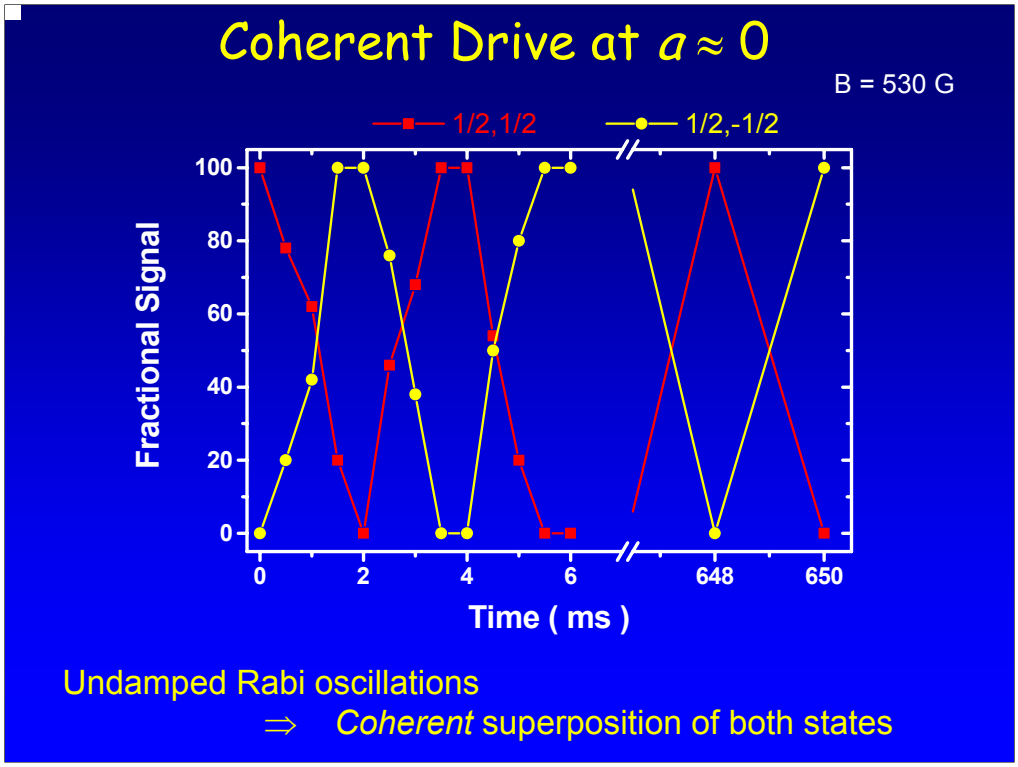

As said previously, ultracold fermions will not interact unless they are in an *incoherent* superposition. We found that making such a superposition was not trivial to create. Starting with all the atoms in the lowest sublevel (F=½, m_F=½), we used *rf* to drive the transition to the next sublevel (F=½, m_F=-½). We found that the population oscillated coherently for many seconds, without decohering for the lifetime of the atoms in the trap (~20 s).

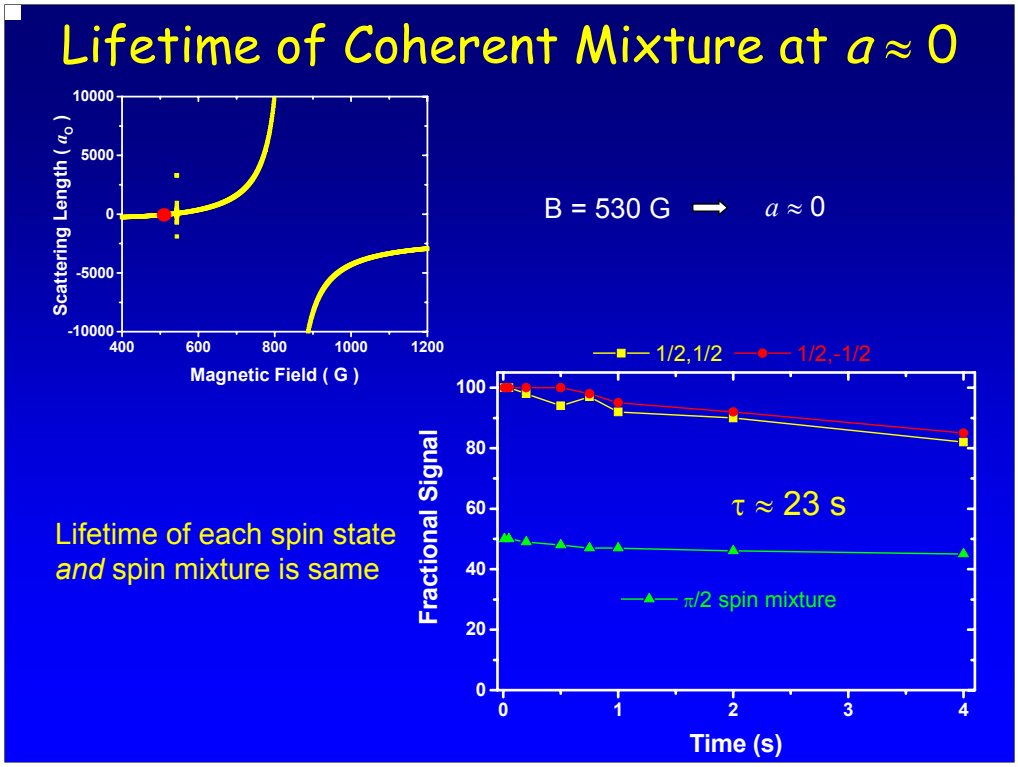

We tuned the magnetic field to 530 G, where $a \approx 0$, and created a 50% mixture in each spin state. The lifetime of the mixture, was the same as a pure states.

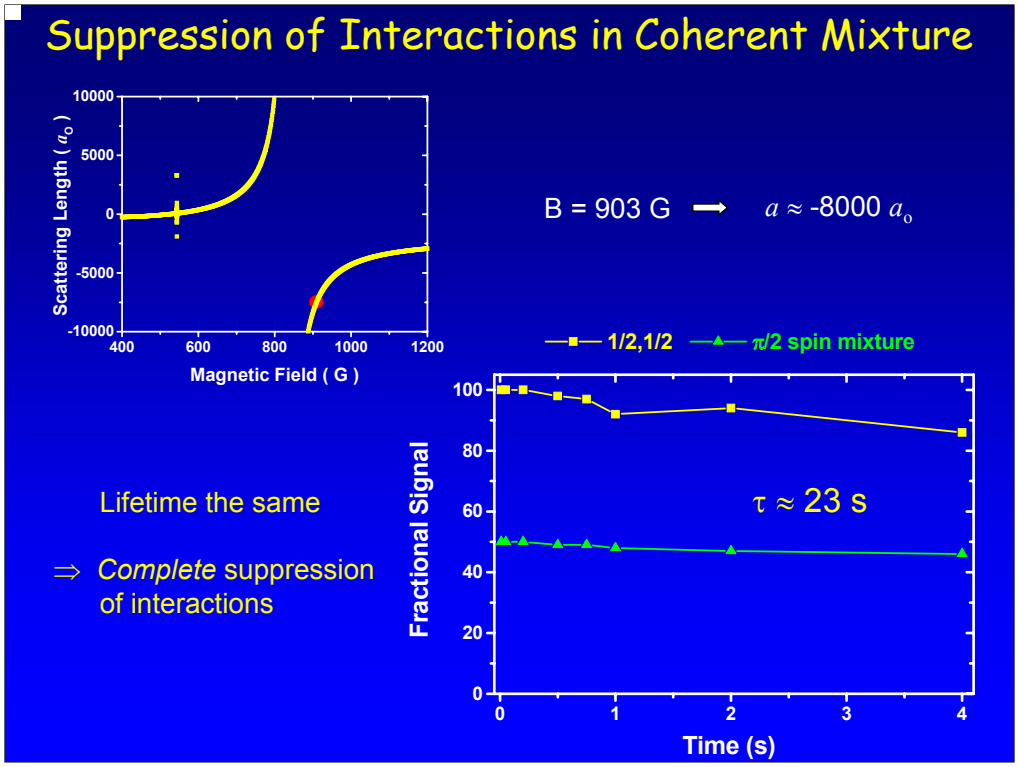

Next, we tuned the field to 903 G where the scattering length has an extremely large magnitude. In this case, we would expect an interacting gas to have a very short lifetime in the trap because as the atoms elastically scatter and evaporate out of the short trap. Incredibly, we again find the lifetime of the 50/50 mixture is the same as that of a pure state. This demonstrates that each atom in the coherently prepared mixture is identical and again, Fermi statistics prevents interaction. We believe that the long coherence time are evidence of extreme magnetic field homogeneity.

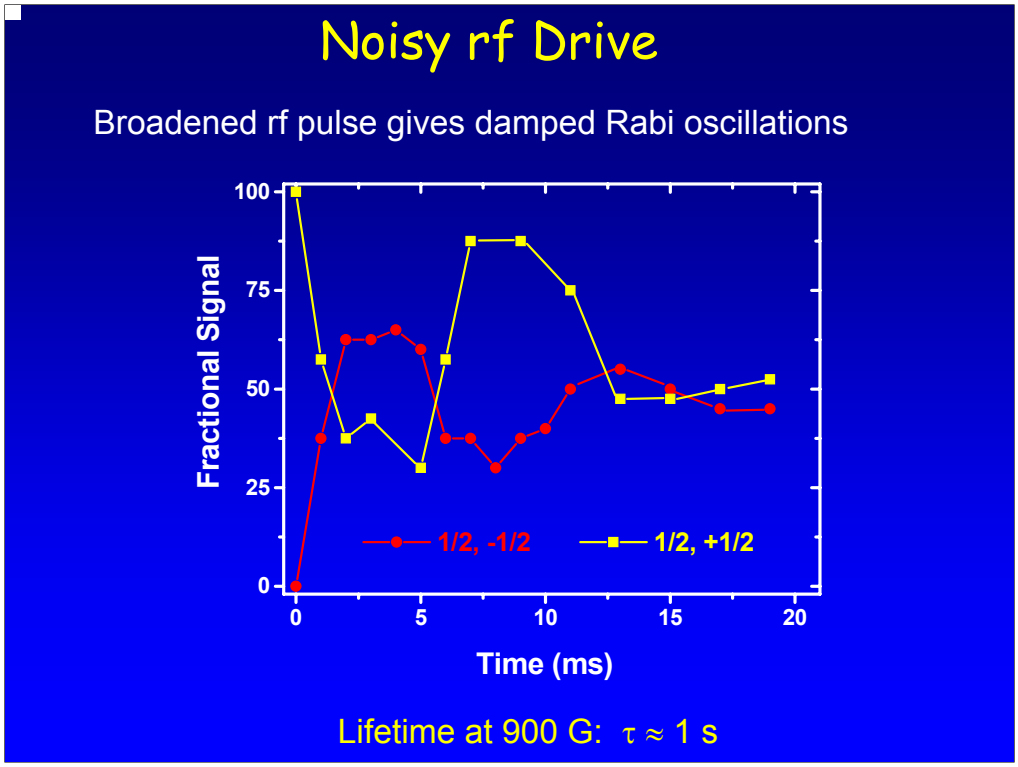

An rf field in which white noise is added to spectrally broaden it results in damped Rabi oscillations. Although such dynamics are indicative of decoherence they can also occur in a completely coherent system, such as this one. We would expect that the coherent Rabi oscillations would revive sometime after the initial damping at 20 ms.

Summary

- Dual evaporation gives 50 million fermions at $T = 0.1\ T_F$
- Demonstrated suppression of interactions by coherent superposition - applicable to atomic clocks
- Looking for evidence of Cooper pairing and superfluidity

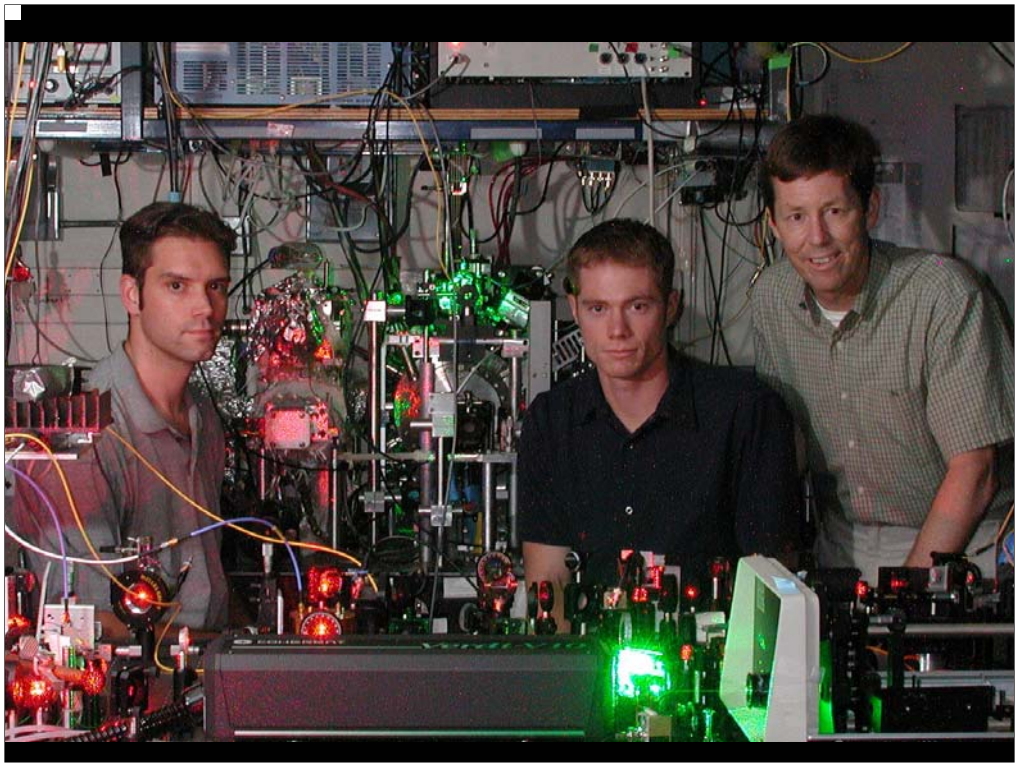

The two guys, left and center, are Kevin Strecker and Guthrie Partridge, who performed the experiments discussed in this talk.

Compact Femtosecond Laser-based Optical Synthesizer for Precision Measurements and Atomic Clocks in the Optical Domain

Scott Diddams & Leo Hollberg
NIST-Boulder

Experiments with ultracold quantum-degenerate fermionic lithium atoms

Wolfgang Ketterle

Research Laboratory for Electronics, MIT-Harvard Center for Ultracold Atoms, and Department of Physics
Massachusetts Institute of Technology, Cambridge, MA 02139, USA
e-mail: ketterle@mit.edu

This article summarizes recent work at MIT on quantum-degenerate Fermi gases. An overview of this work was presented at the NASA workshop in Oxnard on 4/14/2003.

1. Two species mixture of quantum degenerate Bose and Fermi gases

Experimental methods of laser and evaporative cooling, used in the production of atomic Bose-Einstein condensates have recently been extended to realize quantum degeneracy in trapped Fermi gases [1]. Fermi gases are a new rich system to explore the implications of Pauli exclusion on scattering properties of the system, and ultimately fermionic superfluidity.

We have produced a new macroscopic quantum system, in which a degenerate ^{6}Li Fermi gas coexists with a large and stable ^{23}Na BEC [2]. This was accomplished using inter-species sympathetic cooling of fermionic ^{6}Li in a thermal bath of bosonic ^{23}Na. We have achieved high numbers of both fermions ($>10^5$) and bosons ($>10^6$), and ^{6}Li quantum degeneracy corresponding to one half of the Fermi temperature. This is the first time that a Fermi sea was produced with a condensate as a "refrigerator".

Low rates for both intra- and inter-species inelastic collisions result in a lifetime longer than 10 s. Hence, in addition to being the starting point for studies of the degenerate Fermi gas, this system shows great promise for studies of degenerate Bose-Fermi mixtures, including collisions between the two species, and of limitations to the sympathetic cooling process.

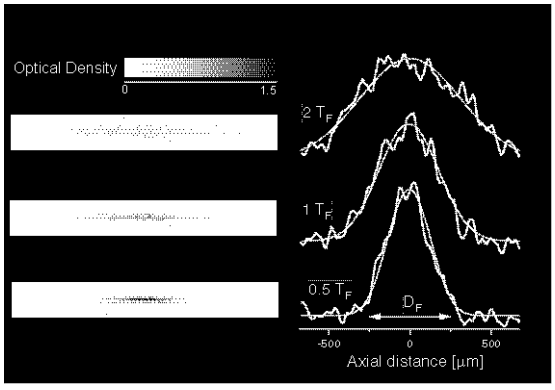

Onset of Fermi degeneracy. Three pairs of images (top to bottom) correspond to T/T_F= 2, 1, and 0.5. (a) Column densities of the ^{6}Li cloud were recorded by absorption imaging. (b) Axial line density profiles and the Fermi-Dirac fits to the data are plotted. The arrow indicates the size of the Fermi diameter, D_F, which is the diameter of the cloud at zero Kelvin.

2. Decay of an ultracold fermionic lithium gas near a Feshbach resonance

The interactions between atoms can be strongly modified by tuning magnetic fields to Feshbach resonances where a molecular state has the same energy as the colliding atoms.

For degenerate Fermi gases, such control over the interaction strength is crucial in the search for a superfluid phase transition. Otherwise, the phase transition temperatures are too low to be experimentally accessible. Near Feshbach resonances, the enhancement of the scattering length is usually accompanied by enhanced inelastic collisions, which lead to rapid trap loss. We have performed the first study of inelastic collisions in a fermionic system near a Feshbach resonance. We have observed resonant magnetic field dependent inelastic decay of an ultracold, optically trapped spin mixture of ^{6}Li [3].

The spin mixture of the two lowest hyperfine states showed two decay resonances at 550 G and 680 G. The feature near 680 G may be related to the long-predicted Feshbach resonance around 800 G. The resonance at 550G was unexpected, but new theoretical calculations have now identified it as an additional Feshbach resonance [4], which was not found in previous calculations. Even on resonance, the observed decay happened on a time scale longer than the trap oscillation time, the time for elastic collisions, and the expected sub-millisecond time needed for the formation of Cooper pairs.

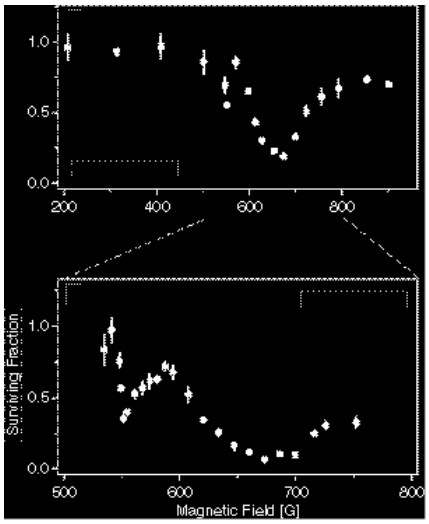

Magnetic field dependence of inelastic decay of lithium in a 50%-50% mixture of the lowest two hyperfine states. The fraction of the atoms remaining after a 500 ms magnetic field pulse is shown (upper graph). The two resonances are shown in more detail for 2 s magnetic field pulses (lower graph).

3. Radio-Frequency Spectroscopy of Ultracold Fermions

Radio-frequency techniques were used to study ultracold fermions [5]. By starting with a sample in one quantum state (state 2) and driving it to another state (state 3) we verified the prediction of the absence of mean-field "clock "shifts, the dominant source of systematic error in current atomic clocks based on bosonic atoms. This absence is a direct consequence of fermionic antisymmetry which prevents two atoms in the same state to interact with contact interactions.

Resonance shifts proportional to interaction strengths were observed in a three-level system when the transition between states 2 and 3 was driven in the presence of atoms in a third state (state 1). When the interactions were weak, the observed shifts agreed with theoretical calculations. However, in the strongly interacting regime, these shifts became very small, reflecting the quantum unitarity limit and many-body effects. This insight into an interacting Fermi gas is relevant for the quest to observe superfluidity in this system.

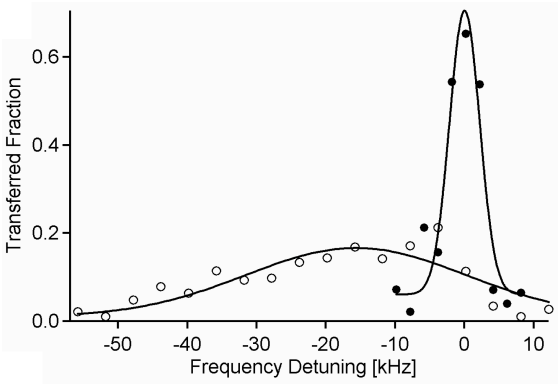

Measurement of the mean-field energy in an interacting Fermi gas. The fraction of atoms transferred by the radio-frequency pulse from state 2 to state 3.with atoms in state 1absent (solid circles)and present (open circles). The mean-field shift due to the presence of atoms in state 1 is computed from Gaussian fits to the data (solid lines).

4. Fifty-fold improvement in the number of quantum degenerate fermionic atoms

For a long time, the cooling of Fermi gases was lagging behind the studies of atomic Bose-Einstein condensates (BECs) due to the complexity of cooling methods. The Pauli exclusion principle prohibits elastic collisions between identical fermions at ultra-low temperatures, and makes evaporative cooling of spin-polarized fermionic samples impossible. For this reason, cooling of fermions must rely on some form of mutual or sympathetic cooling between two types of distinguishable particles. A key element in fermion cooling is the design of better "refrigerators" for sympathetic cooling.

We have realized evaporative cooling of sodium in the upper hyperfine state (F=2) and achieved Bose-Einstein condensates in this state by direct evaporation. Sympathetic cooling of lithium with that cloud decreased losses due to inelastic collisions encountered in earlier experiment with sodium in the lower (F=1) state.

This further cooling of the lithium resulted in the production of degenerate Fermi samples comparable in size with the largest alkali BECs [6]. We successfully cooled up to 7 X 10^7 magnetically trapped ^{6}Li atoms to below half the Fermi temperature (T_F), an improvement in atom number by a factor of 50 over the largest previously reported Fermi sea. Further, in samples containing up to 3 X 10^7 atoms, we observed temperatures as low as 0.05 T_F, the lowest ever achieved. At these temperatures, the fractional occupation of the lowest energy state differs from unity by less than 10^{-8}.

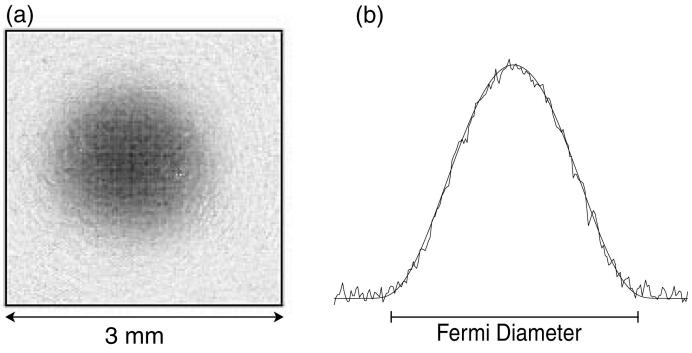

Large and ultra-degenerate Fermi sea. (a) Absorption image of 3 _ 10^7 ^{6}Li atoms released from the trap and imaged after 12 ms of free expansion. (b) Axial (vertical) line density profile of the cloud in (a). A semiclassical fit (thin line) yields a temperature T = 93 nK= 0.05 T_F . At this temperature, the high-energy wings of the cloud do not extend visibly beyond the Fermi energy, indicated in the figure by the momentum-space Fermi diameter.

5. Collisions in zero temperature Fermi gases

The smoking gun of Bose-Einstein condensation has been the anisotropic "superfluid" expansion of elongated condensates released from the trap. Similarly, superfluid Fermi gas would show anisotropic expansion due to superfluid hydrodynamics [7]. A recent observation of anisotropic expansion of an ultracold, interacting, two-spin fermionic mixture [8] has created considerable excitement and raised the question under what conditions is this expansion a signature of fermionic superfluidity and not of collisional hydrodynamics.

We examined the collisional behavior of two-component Fermi gases released at zero temperature from a harmonic trap [9]. Using a phase-space formalism to calculate the collision rate during expansion, we find that Pauli blocking plays only a minor role for momentum changing collisions. As a result, for a large scattering cross-section, Pauli blocking will not prevent the gas from entering the collisionally hydrodynamic regime. In contrast to the bosonic case, hydrodynamic expansion at very low temperatures is therefore not evidence for fermionic superfluidity.

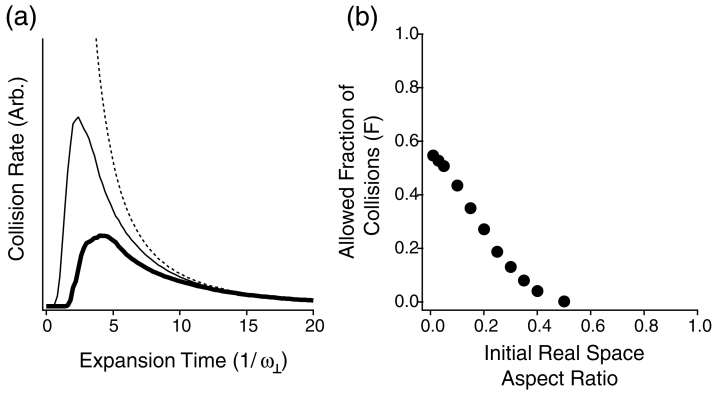

(a) Collision rate as a function of expansion time in the perturbative approximation for an initial aspect ratio of 0.03. Dashed line: total classical collision rate, thin line: classical rate for momentum changing collisions, thick line: collision rate for fermions. (b) Allowed fraction of collisions for a zero-temperature two-spin Fermi gas. For an initial aspect ratio of 0.05, the fraction is 0.5, and approaches 0.55 for large anisotropy.

6. Spectroscopic insensitivity to cold collisions in a two-state mixture of fermions

We have experimentally addressed the relation between coherence and spectroscopic measurements in a binary mixture of ultracold fermions. We demonstrated that shifts of spectroscopic lines are absent even in a fully decohered binary mixture, in which the particles are distinguishable, and the many-body mean-field energy in the system has developed [10]. We theoretically showed that this is a direct consequence of the coherent

nature of the RF excitation, and is not dependent on the coherence of the sample on which spectroscopy is performed. Our calculation intuitively explains both our results for fermions, and previous results for bosons obtained in Boulder [11].

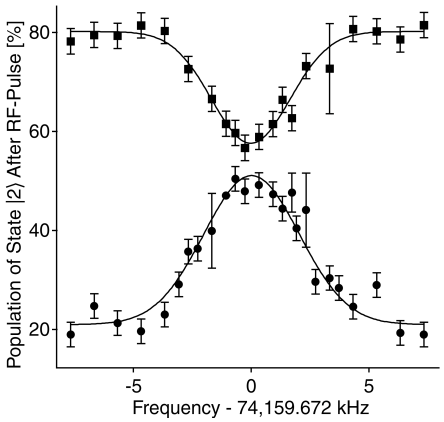

Absence of mean-field shift of an RF transition in a binary Fermi system. The resonance curves were measured for fully decohered 80%/20% two-state mixtures of fermions. The measured frequency difference between the two lines is (34 ± 146) Hz, even though a simple mean-field model would predict a splitting of 20 kHz.

1. B. DeMarco and D.S. Jin, Science **285**, 1703 (1999).
2. Z. Hadzibabic, C.A. Stan, K. Dieckmann, S. Gupta, M.W. Zwierlein, A. Görlitz, and W. Ketterle, Phys. Rev. Lett. **88**, 160401 (2002).
3. K. Dieckmann, C.A. Stan, S. Gupta, Z. Hadzibabic, C. Schunck, and W. Ketterle, Phys. Rev. Lett. **89**, 203201 (2002).
4. K.M. O'Hara, S.L. Hemmer, S.R. Granade, M.E. Gehm, J.E. Thomas, V.Venturi, E. Tiesinga, and C.J. Williams, Phys. Rev. A **66**, 041401(R) (2002).
5. S. Gupta, Z. Hadzibabic, M.W. Zwierlein, C.A. Stan, K. Dieckmann, C.H. Schunck, E.G.M.v. Kempen, B.J. Verhaar, and W. Ketterle, Science **300**, 1723 (2003).
6. Z. Hadzibabic, S. Gupta, C.A. Stan, C.H. Schunck, M.W. Zwierlein, K. Dieckmann, and W. Ketterle, preprint cond-mat/0306050.
7. C. Menotti, P. Pedri, and S. Stringari, Phys. Rev. Lett. **89**, 250402 (2002).
8. K.M. O'Hara, S.L. Hemmer, M.E. Gehm, S.R. Granade, and J.E. Thomas, Science **298**, 2179 (2002).
9. S. Gupta, Z. Hadzibabic, J.R. Anglin, and W. Ketterle, preprint, cond-mat/0307088.
10. M.W. Zwierlein, Z. Hadzibabic, S. Gupta, and W. Ketterle, preprint cond-mat/0306627.
11. D.M. Harber, H.J. Lewandowski, J.M. McGuirk, and E.A. Cornell, in *Proceedings of the XVIII International Conference on Atomic Physics*, edited by H.R. Sadeghpour, E.J. Heller, and D.E. Pritchard (World Scientific, Cambridge, Massachusetts, 2003) p. 3.

New Experiment to Measure the Electron Electric Dipole Moment

Melanie Kittle
University of Texas at Austin

An electron can possess an electric dipole moment (edm) only if time reversal symmetry (T) is violated. No edm of any particle has yet been discovered. CP-violation, equivalent to T-violation by the CPT theorem, does occur in Kaon decays and can be accounted for by the standard model. However, this mechanism leads to an electron edm d_e of the order of
10^{-38} e cm, whereas the current experimental bound on d_e is about 10^{-27} e cm. However, well-motivated extensions of the standard model such as supersymmetric theories do predict that d_e could be as large as the current bound. In addition, CP violation in the early universe is required to explain the preponderance of matter over anti-matter, but the exact mechanism of this CP violation is unclear. For these reasons, we are undertaking a new experimental program to determine d_e to an improved accuracy of 10^{-29} e cm. Our experiment will use laser-cooled, trapped Cesium atoms to measure the atomic edm d_{Cs} that occurs if d_e is not zero. In order to do this, we will measure the energy splitting between the atoms' spin states in parallel electric and magnetic fields. The signature of an edm would be a linear dependence of the splitting on the electric field E due to the interaction - d_{Cs}•E. Our measurement will be much more sensitive than previous measurements because atoms can be stored in the trap for tens of seconds, allowing for much narrower Zeeman resonance linewidths. Also, our method eliminates the most important systematic errors, proportional to atomic velocity, which have limited previous experiments. In this presentation, we will describe the design of our new apparatus, which is presently under construction. An important feature of our experimental apparatus is that magnetic field noise will be suppressed to a very low value of the order of 1 $fT/(Hz)^{1/2}$. This requires careful attention to the Johnson noise currents in the chamber, which have not been important in previous experiments. In addition we will present estimates of the limits of the various errors that we expect for our experiment.

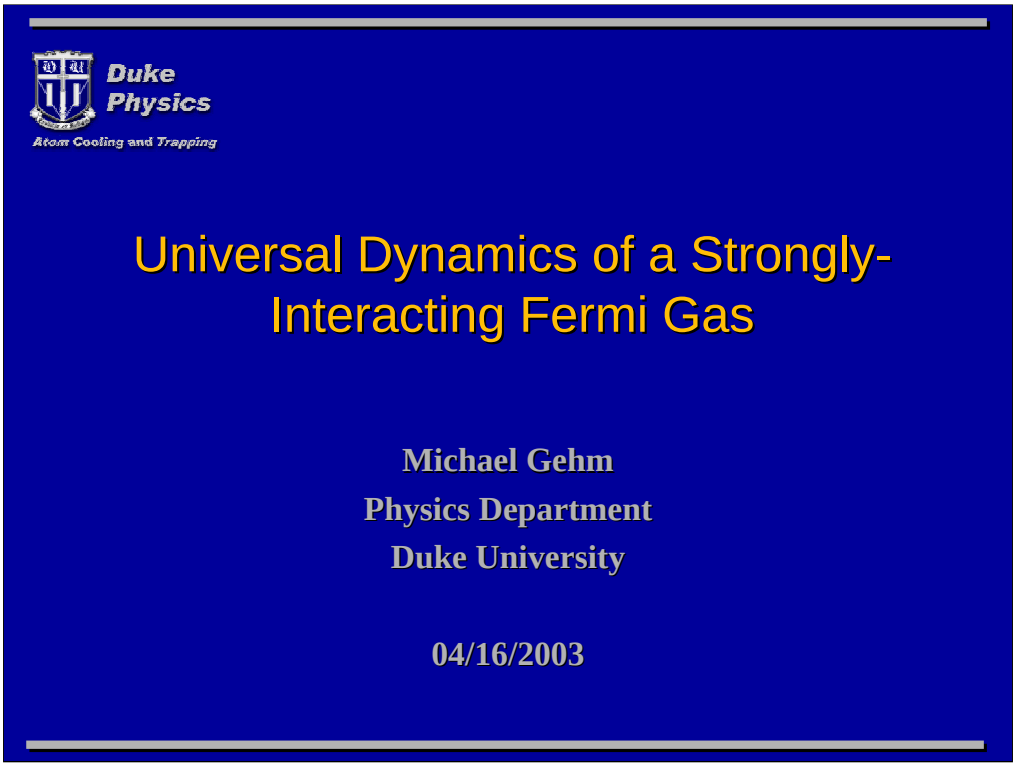
Duke
Physics
Atom Cooling and Trapping
Universal Dynamics of a Strongly-Interacting Fermi Gas
Michael Gehm
Physics Department
Duke University
04/16/2003

Duke Physics
Atom Cooling and Trapping

Outline

- Current work in atomic DFGs
- New frontier: Universal Behavior in Strongly-Interacting Fermi Gases
- Free Expansion Experiment
- Extraction of a Universal Parameter
- Summary

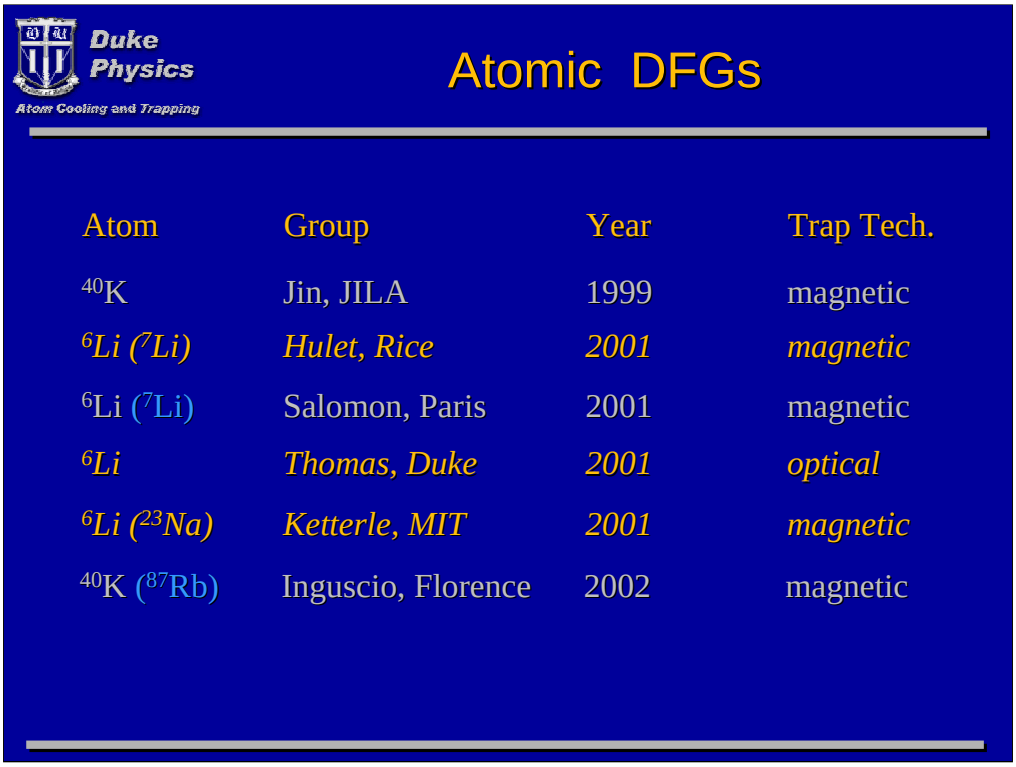

Over the past several years, there have been a number of atomic degenerate Fermi gases created around the world. In every case, these degenerate gases were produced via evaporative cooling in a neutral atom trap.

At JILA and in our own work at Duke, the evaporation is driven by collisions between two hyperfine states of a single atomic species. The other experiments use "sympathetic cooling" where the fermionic species shares the trap with a bosonic partner in thermal equilibrium.

The NASA fundamental physics in microgravity program is well represented in the field---the Rice, Duke and MIT groups are all speaking at this conference.

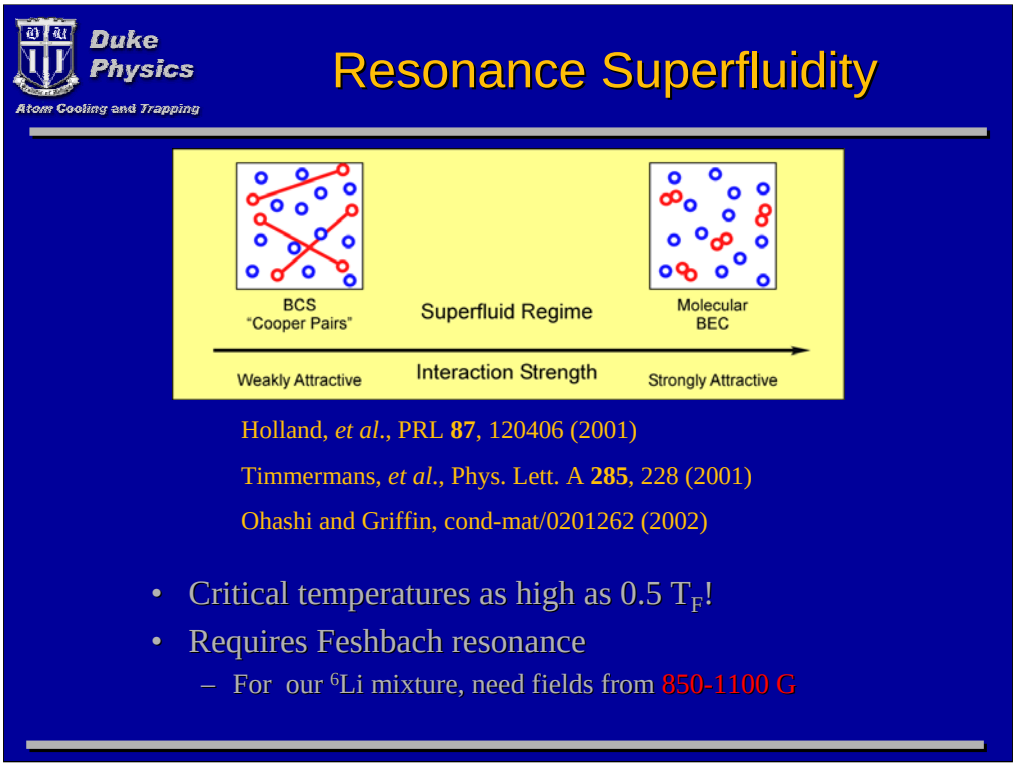

An exciting motivator in the field of atomic Fermi-physics is the possibility, first suggested only a few years ago, that the superfluid transition temperature might be extraordinarily high in the region where the interatomic interactions are enhanced by a Feshbach resonance. The system characterized by this transition lies in the "cross-over region" between weakly-bound cooper pairs and a BEC of tightly-bound molecular dimers.

The transition temperature for a harmonically-trapped degenerate gas of fermions is predicted to be as high as half of the Fermi temperature (several orders of magnitude larger than the transition temperature in metallic superconductors).

In ^{6}Li, our atom of choice, to access the resonance needed for this effect requires magnetic fields in the range of 850-1100 G.

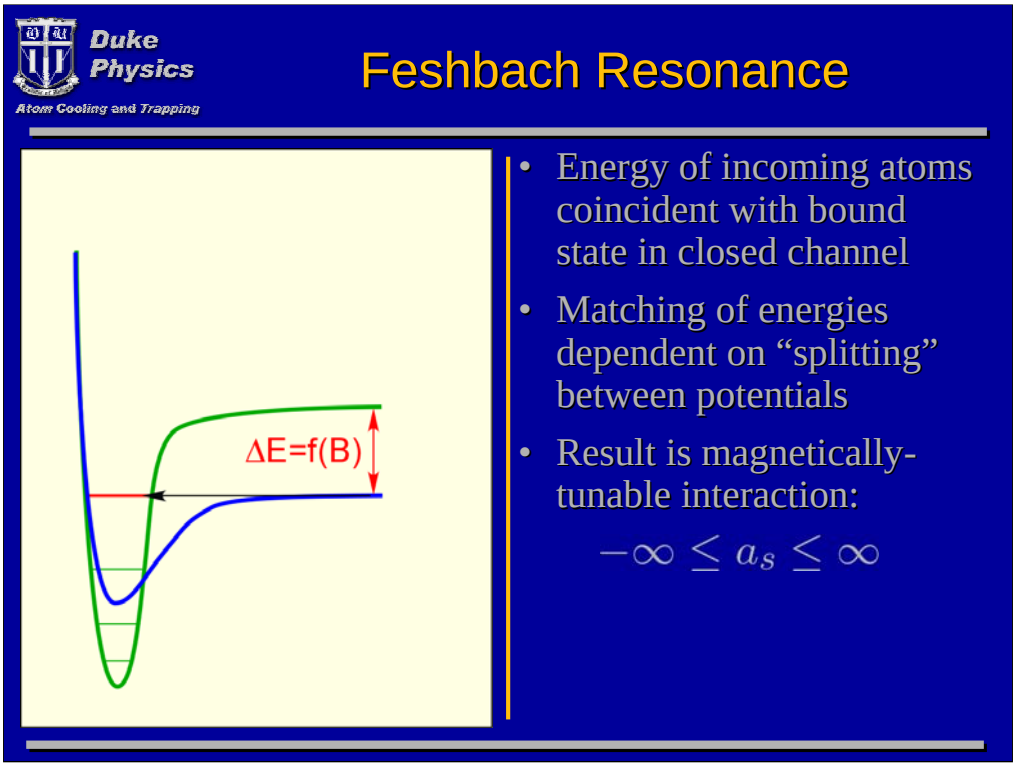

Strong interatomic interactions are produced in the system by a Feshbach resonance. In a Feshbach resonance, the energy of the colliding atoms is energetically tuned into resonance with a bound state on a closed exit channel. In ^{6}Li, the two relevant channels are the single and triplet potentials. The triplet state tunes in a magnetic field, so the relative spacing between the potentials can be varied by changing an externally-applied magnetic field.

The result is a magnetically-tunable interaction, characterized by the zero-energy s-wave scattering length, which can take on all values.

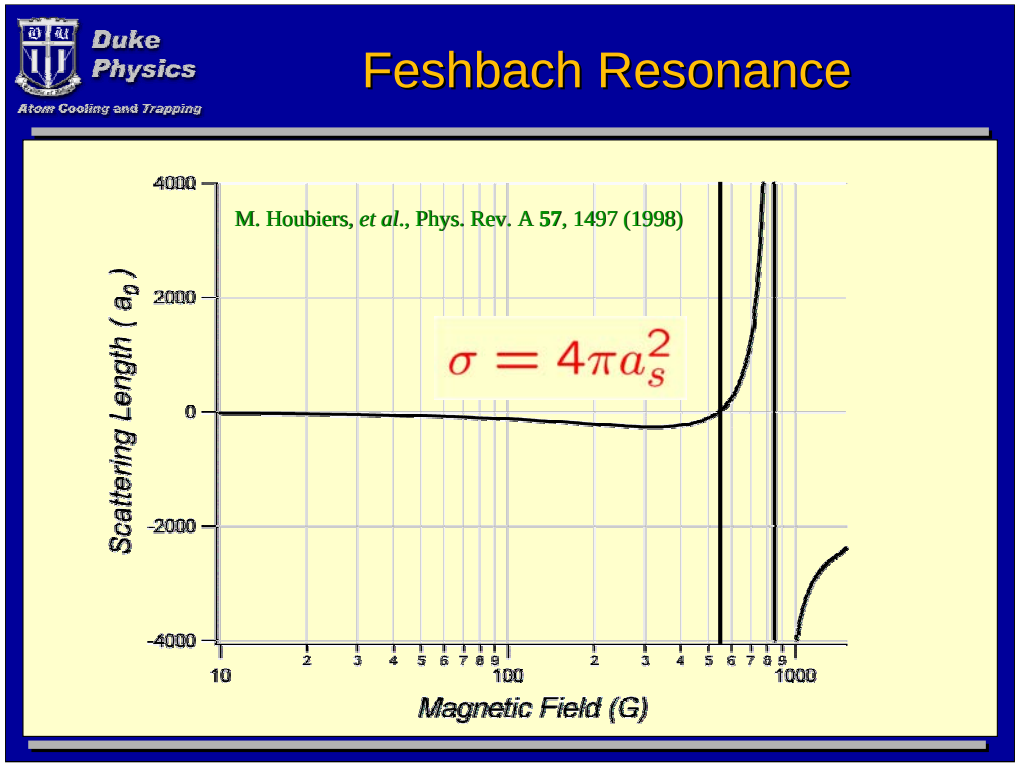

This plot shows the s-wave scattering length as a function of magnetic field for the two lowest hyperfine groundstates of ^{6}Li. Two Feshbach resonances are shown, a narrow resonance at approximately 550G and a very broad resonance centered near 850 G.

In addition, it is important to note another nice feature of this atomic system---the scattering length, and hence the interactions, are zero at zero magnetic field. Thus we can change from an interacting system to a non-interacting one (or vice-versa) simply by applying or removing a magnetic field.

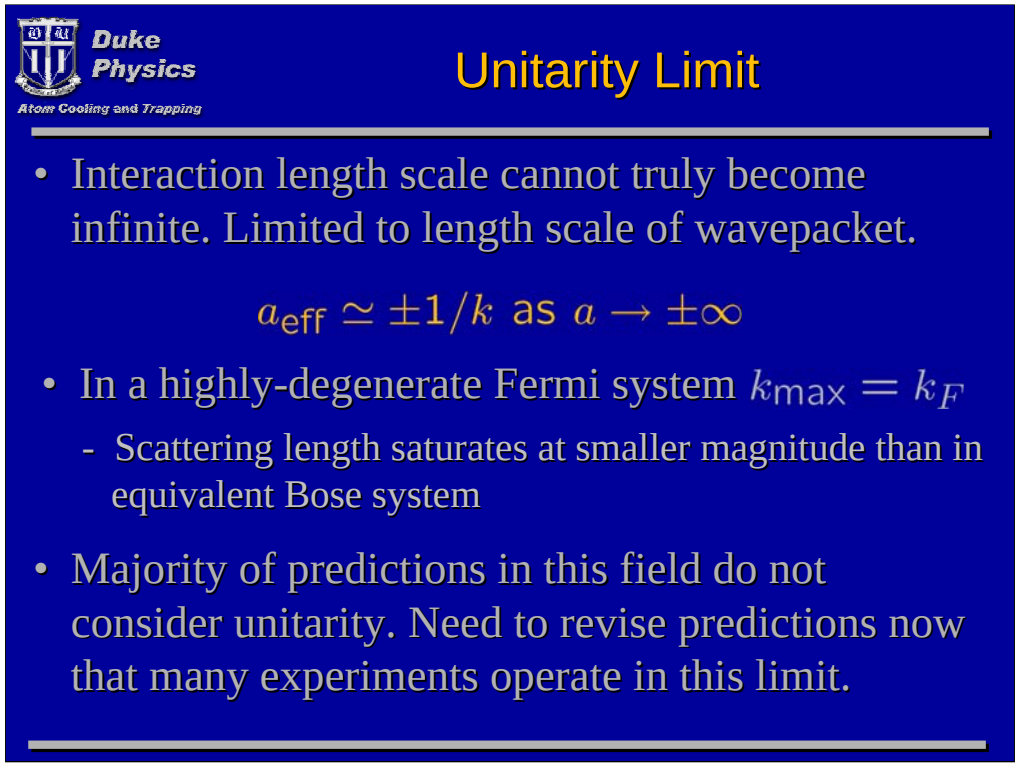

There is, however, a problem with the simplistic view presented so far---it ignores the quantum-mechanical requirement of unitarity.

Because of the requirement of unitarity, the interaction strength cannot truly become infinite. The effective scattering length is, in fact, limited to approximately the inverse of the wavenumber. This has interesting implications in a Fermi system. For a degenerate Fermi system, there will be wavenumbers up to the Fermi wavenumber. In contrast, in a degenerate Bose system, the wavenumbers are all much smaller and correspond to the ground state of the confining potential. This means that the scattering length saturates to a much smaller value in Fermi systems than in Bose systems.

Perhaps because unitarity is not particularly important in Bose systems, many of the early predictions about fermions did not consider this important fact. Now that all the major experiments are operating in regimes where the scattering length is resonantly enhanced, it is crucial to review earlier predictions in light of unitarity.

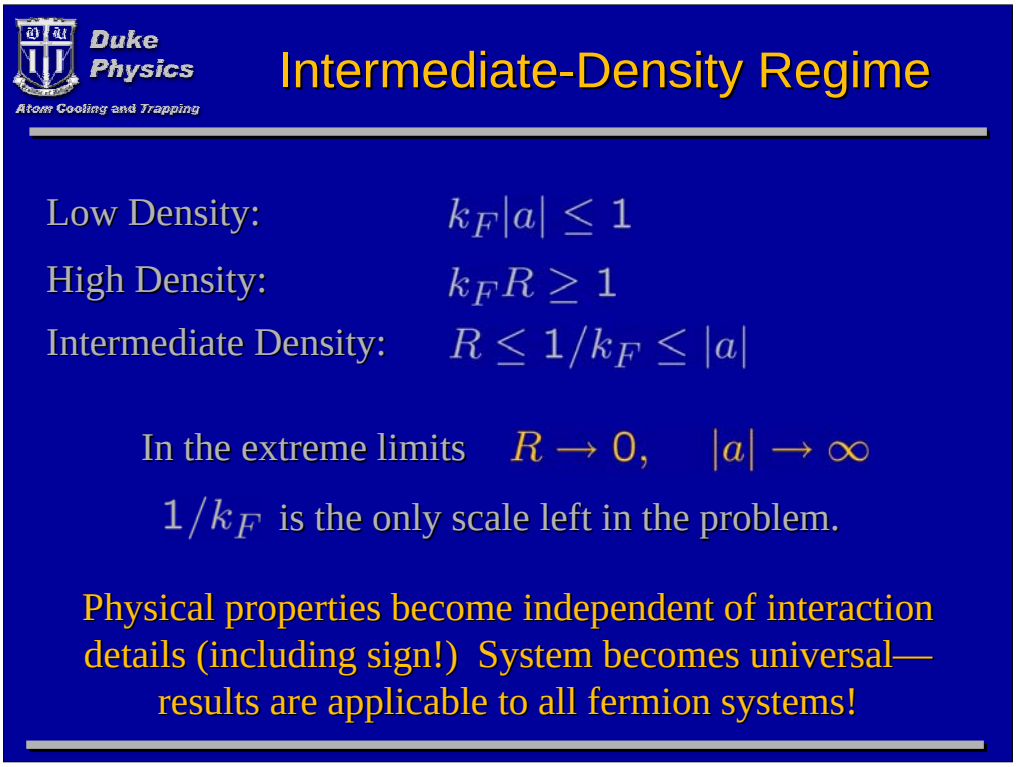

Things become even more interesting when we start to consider many-body effects.

There are two natural limits when discussing these types of systems: the low density limit where the interaction length scale is much smaller than the interatomic spacing, so that many body effects are unimportant, and the high density limit where the interaction length scale is much larger than the range of the interaction potentials, in which case mean-field treatments are excellent approximations.

In the intermediate density regime, neither of these limits apply, and initially one might suspect the system is intractable. However, a very interesting thing happens in this limit. The two length scales of the interaction (the scattering length and the range of the potential) become effectively either infinity or zero---leaving the inverse Fermi wavenumber as the only length scale in the problem

It has been suggested that systems in this regime are universal. The behavior of the system is independent of the details of the interaction and is applicable to all fermion systems.

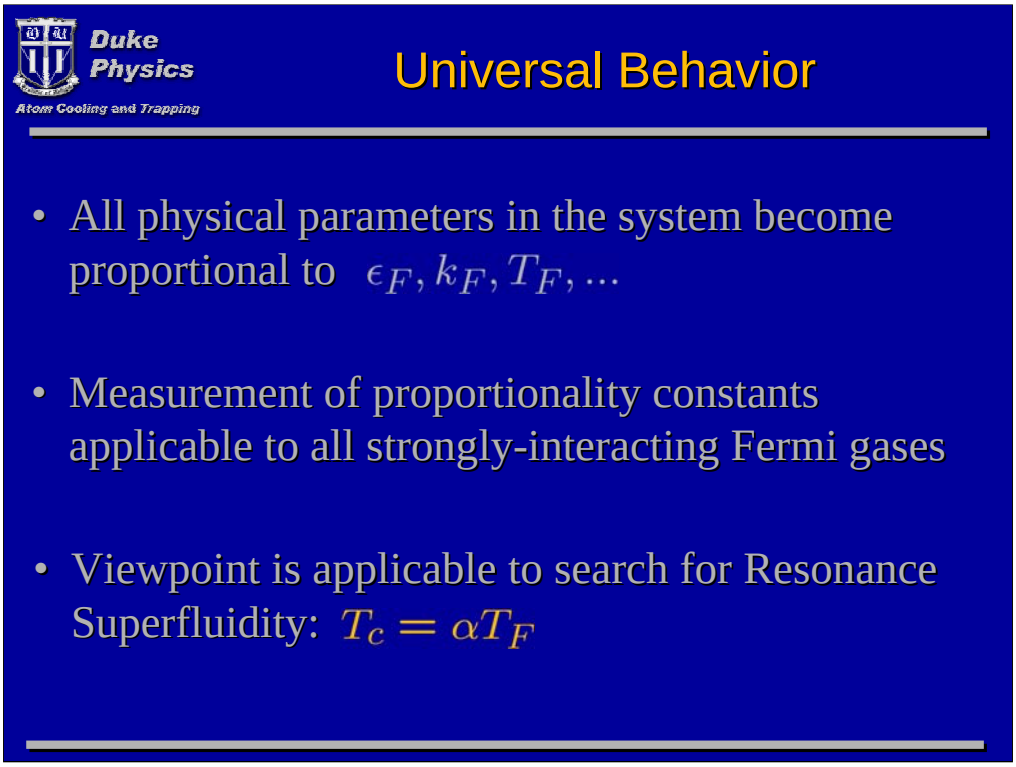

If universal behavior does exist in the intermediate density regime, then all physical parameters become proportional to the Fermi parameters (which themselves are proportional to powers of the Fermi wavenumber).

Measurements of these proportionality constants should then be applicable to all Fermi systems in the intermediate density regime, regardless of the nature of their interactions.

The hunt for resonance superfluidity can then be viewed in this light as a quest to measure the universal proportionality constant between the transition temperature and the Fermi temperature.

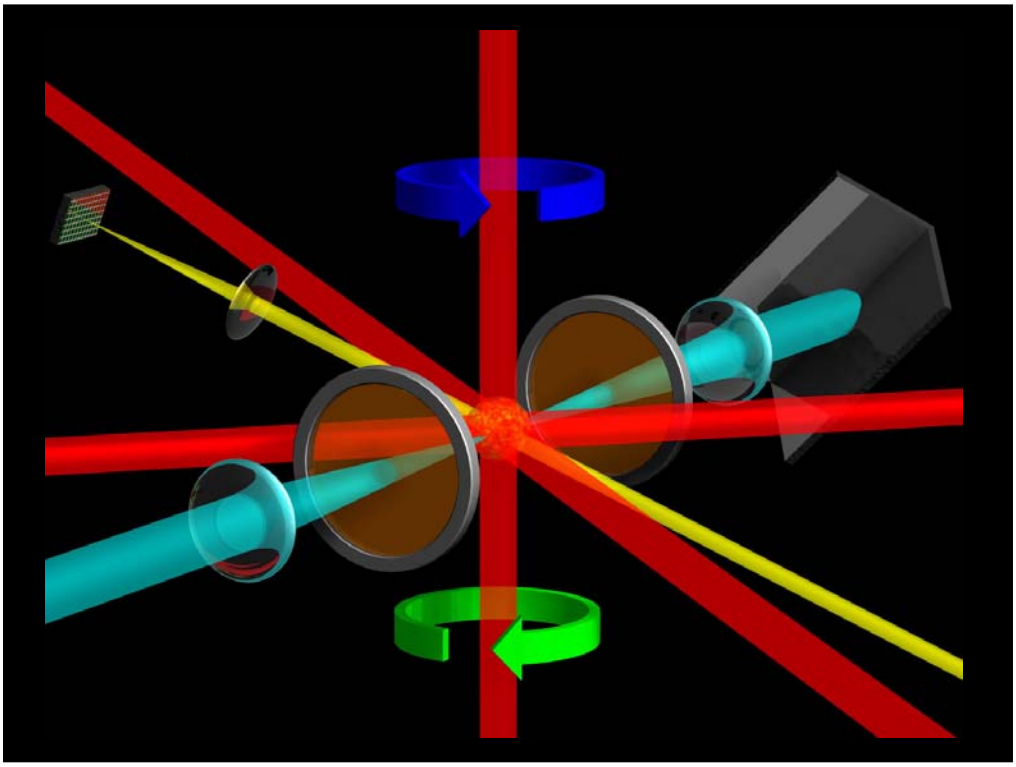

This is a schematic of the sequencing of our experiment.

We create a MOT of ^{6}Li atoms in a UHV system. We then pass a single, focused CO_2 laser beam into the system through ZnSe windows, placing the focus in the center of the MOT.

Several million ^{6}Li atoms at 150 microKelvin are transferred into the dipole force trap formed at the focus, and the MOT beams are extinguished. We change the orientation of one magnetic field coil and apply 900G to the sample, initiating rapid evaporative cooling via the Feshbach resonance.

Once we have a highly degenerate sample, the CO_2 laser is extinguished, allowing the gas to expand. After a desired expansion time, we pass a resonant absorption beam through the cloud and capture the shadow image on a CCD array.

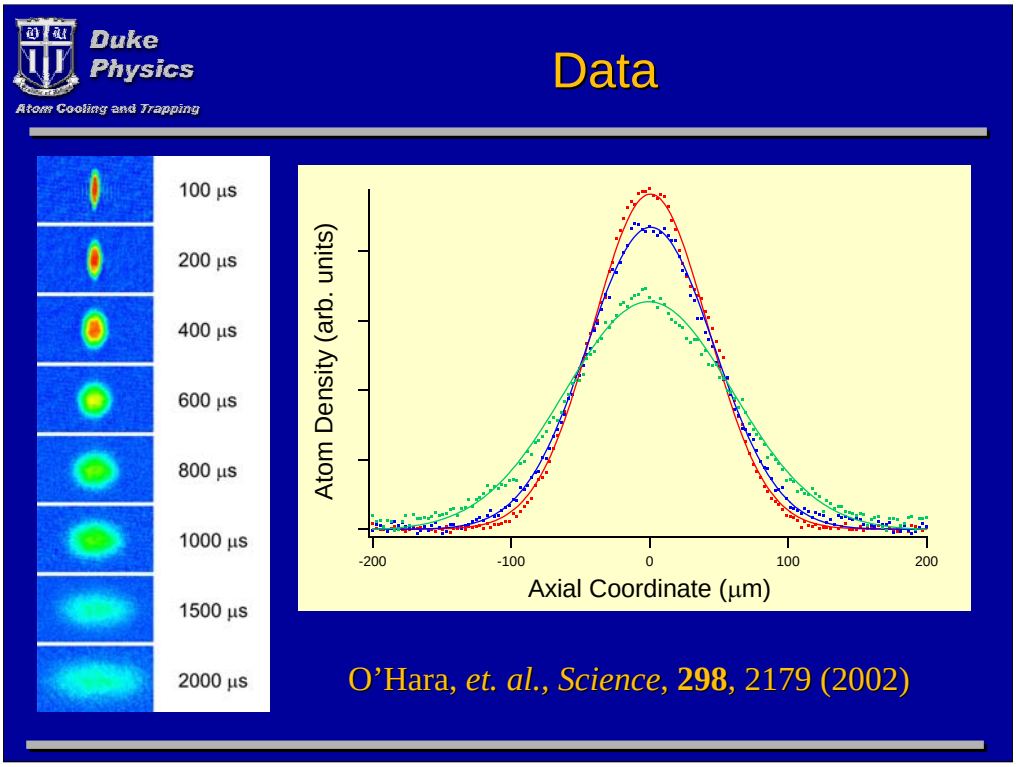

We can release the cloud for varying times and then image using absorption imaging to get the profile of the atomic cloud. The cloud starts in a long, cigar shape and expands in a very anisotropic manner. The narrow direction of the cloud expands quickly, while the initial long direction hardly moves.

This is quite different from the behavior of a non-interacting degenerate Fermi gas, where the isotropy of the momentum would lead to the cloud taking on a spherical shape at long times.

This behavior was initially suggested as a hallmark of superfluidity, although we have shown that it can also arise as a result of unitarity-limited collisions. Thus, while we may have produced a superfluid, we cannot claim so at this point.

The image on the left show the cloud as it expands in time.

The plot on the right shows the expansion of the initially long dimension as a function of time.

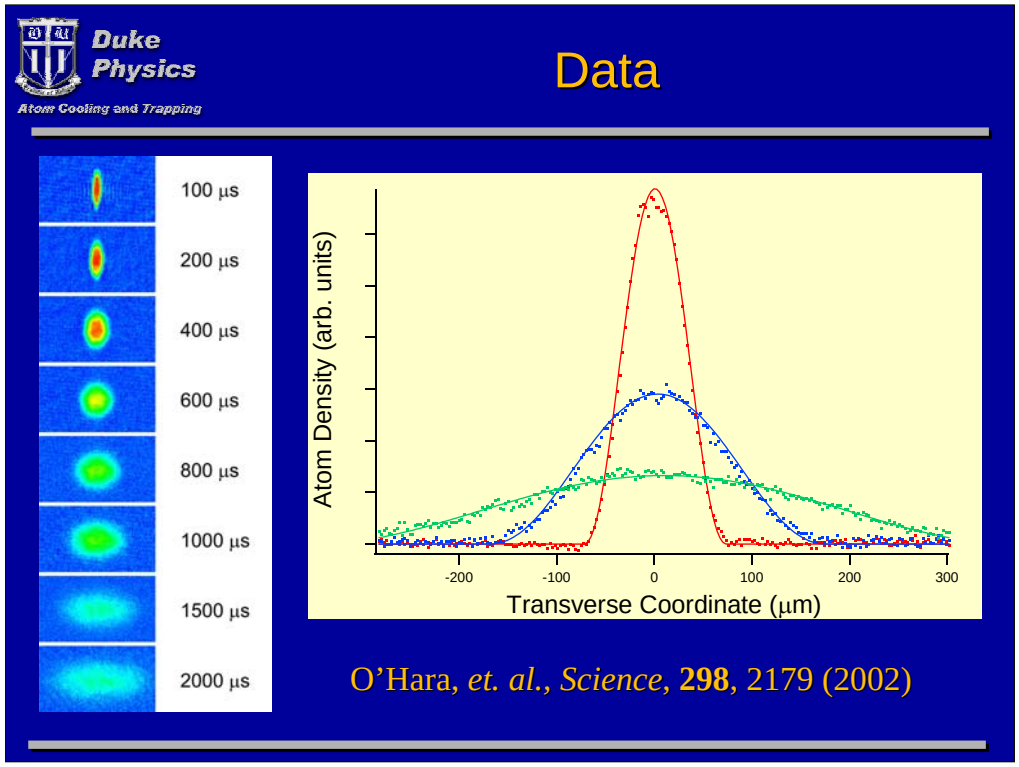

This plot shows the expansion of the initially narrow dimension as a function of time. It is quite clear that this direction expands much more rapidly than the long dimension.

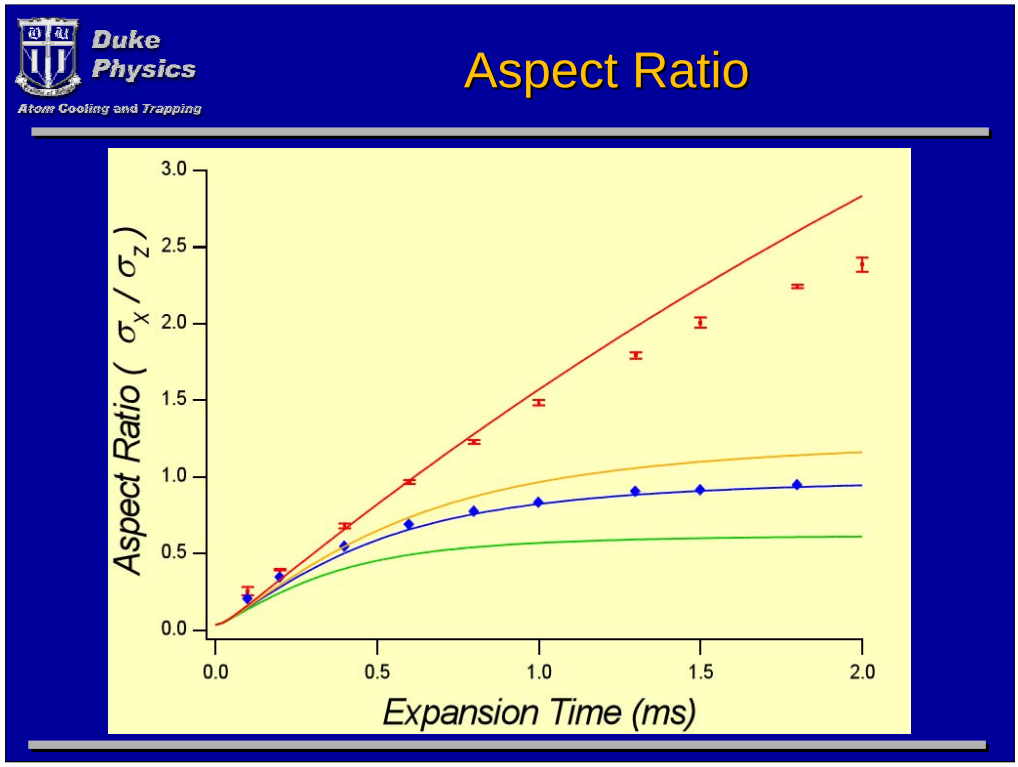

This is a plot of the measured aspect ratio as a function of time (red dots with error bars). The red line which closely approximates the data is for purely hydrodynamic expansion with no free parameters.

The blue data is for a non-interacting cloud. Note that it approaches an aspect ratio of 1 at long time---as we would expect. The curve passing through the blue data is for ballistic expansion with no free parameters..

The orange and green curves show what the expansion would look like if the system were not hydrodynamic, but did have repulsive or attractive mean field interactions, respectively.

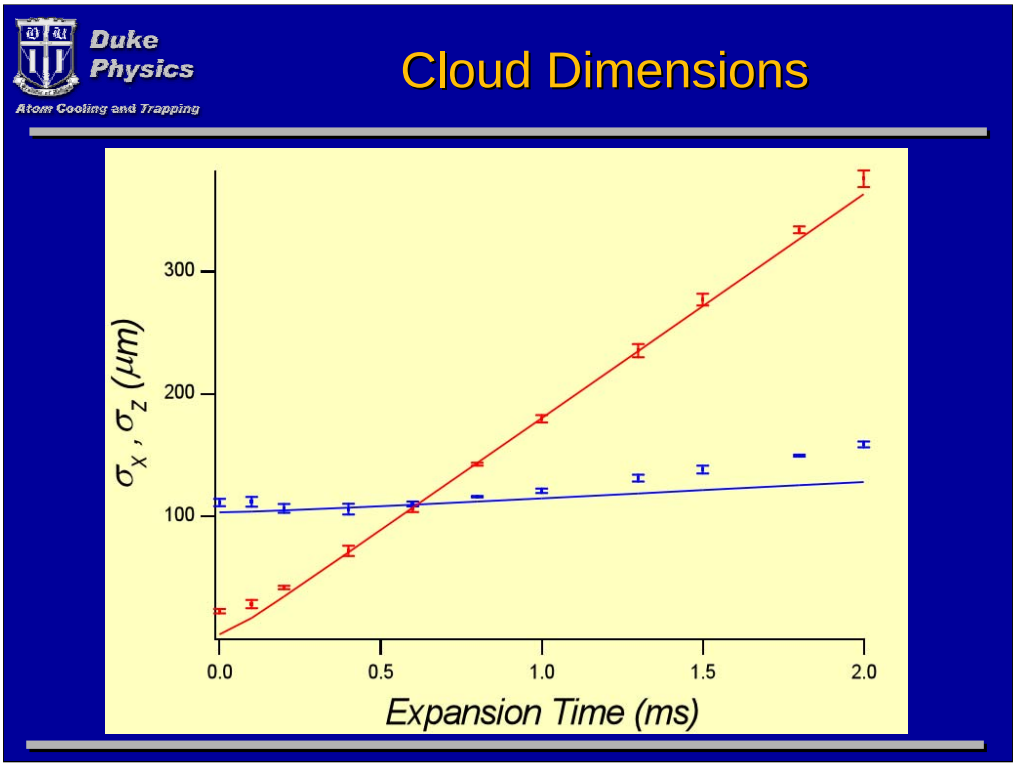

The previous slide showed that hydrodynamic expansion seemed to explain the observed data, however there was a non-negligible deviation at long times. This plot shows the growth of both the initially narrow (red) and initially long dimensions of the cloud.

The solid curves are once again hydrodynamic expansion with no free parameters. It is clear that the radial expansion is well explained by this model. We do not yet have an explanation why the axial dimension of the cloud walks off the curve at long time.

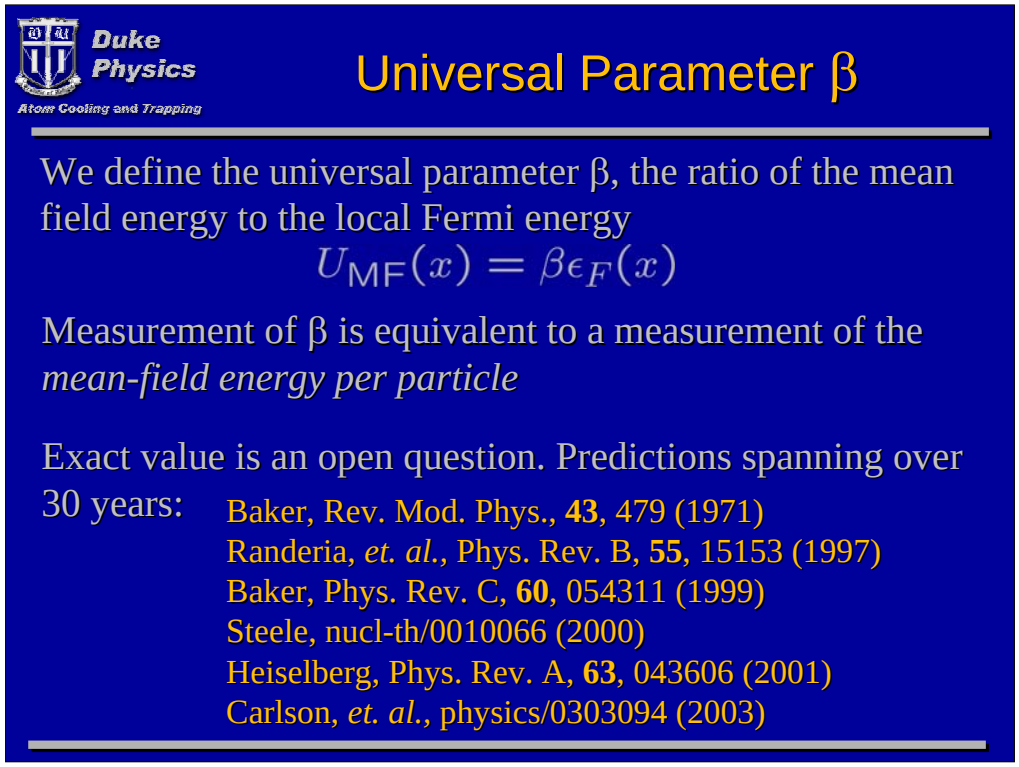

From the expansion data we can make a first measurement of a universal parameter of a degenerate Fermi gas in the intermediate density regime.

In the universal regime, the contribution of the mean field to the chemical potential is proportional to the local Fermi energy. We define the constant of proportionality as β.

Measuring β is equivalent to measuring the mean-field energy per particle in units of the local kinetic energy. This parameter has been the subject of theoretical predictions for well over 30 years.

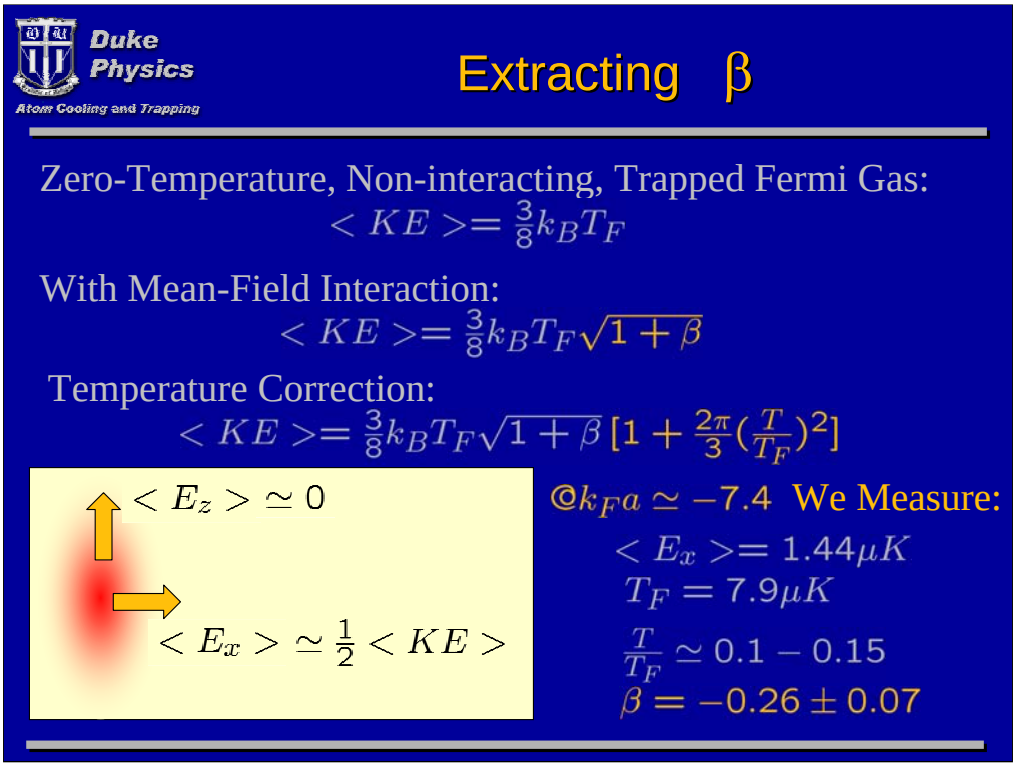

We can extract a measurement for β from our data by relating the kinetic energy of the released cloud to its size after expansion. We account for the finite temperature of the cloud with a Sommerfeld expansion of the density and for the mean-field interaction usng the parameter β.

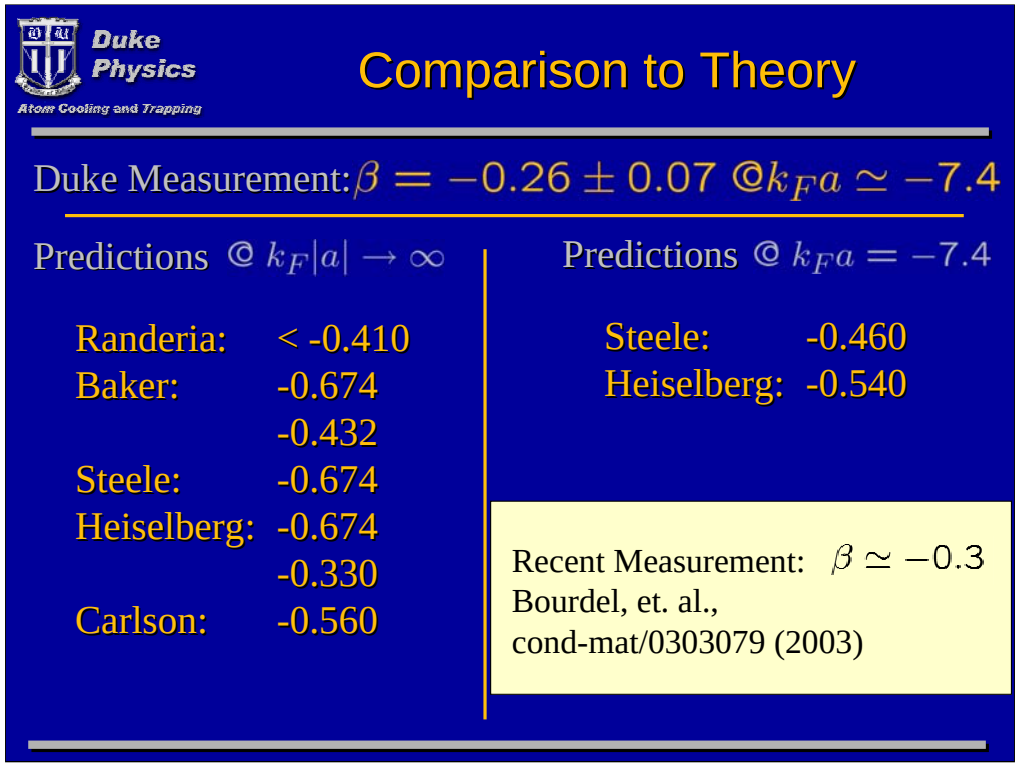

We measure beta=-0.26.

Most theoretical predictions are for the limit where the product of the Fermi wavenumber and the scattering length is infinite. Only a few prediction have explicit k_F a-dependence which we can evaluate.

We find qualitative agreement with the theoretical predictions. Quantitatively, we differ by roughly a factor of two. Where does this discrepancy come from? Recent experiments at ENS in Paris give an answer in close agreement with our measurement. Additionally, some of the best theoretical predictions explicitly ignore terms of order 25%. Further refinements to theory will no doubt help to reconcile the two values. Also, the initial experiments are not as sensitive to beta as we would like. Further experiments should allow us to refine our estimate and reduce the likelihood of systematic errors.

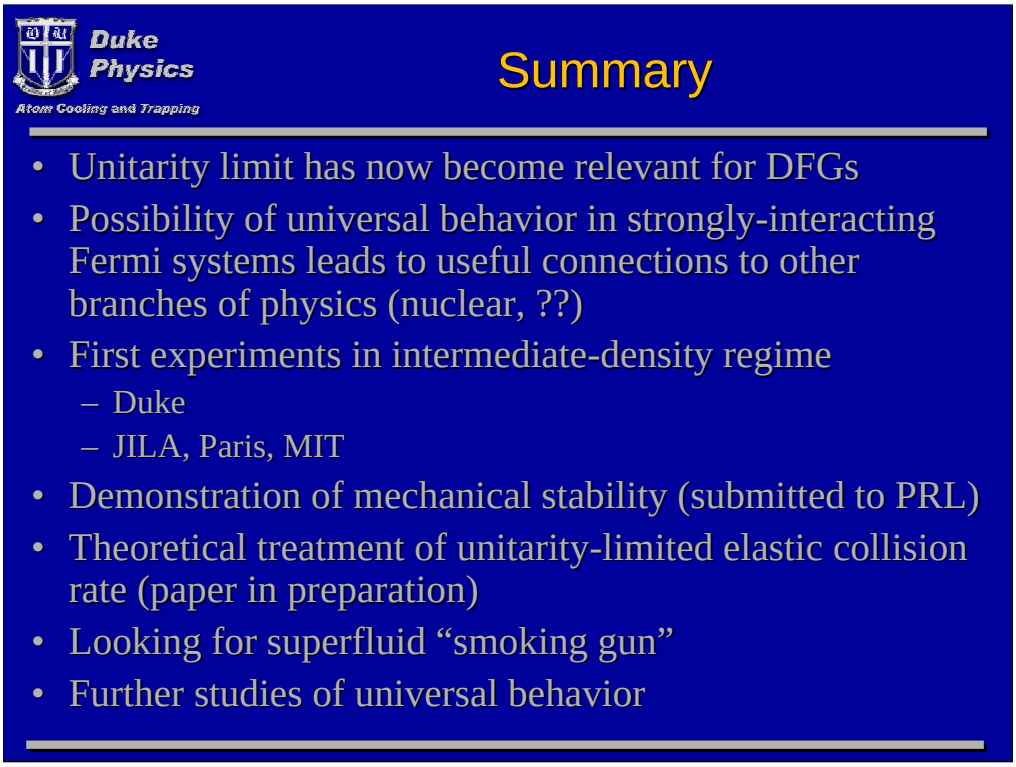

In summary, all the DFG experiments are now working in the strongly-interacting unitarity-limited regime. This limits the applicability of many previous theoretical predictions and may serve as a test for recent theories of strongly-interacting Fermi systems.

An exciting new feature of DFG physics is the possibility of universal behavior in these systems.

The first experiments in the intermediate-density regime have been performed in the past year.

Our work has shown that strongly attractive degenerate Fermi gases are mechanically stable, in contrast to Bose systems. We have also begun to explore the theoretical implications of unitarity on these systems.

We are currently working towards a clear-cut test for superfluidity in our experiment and are beginning further studies of universal behavior.

Duke Physics

Atom Cooling and Trapping

The Team

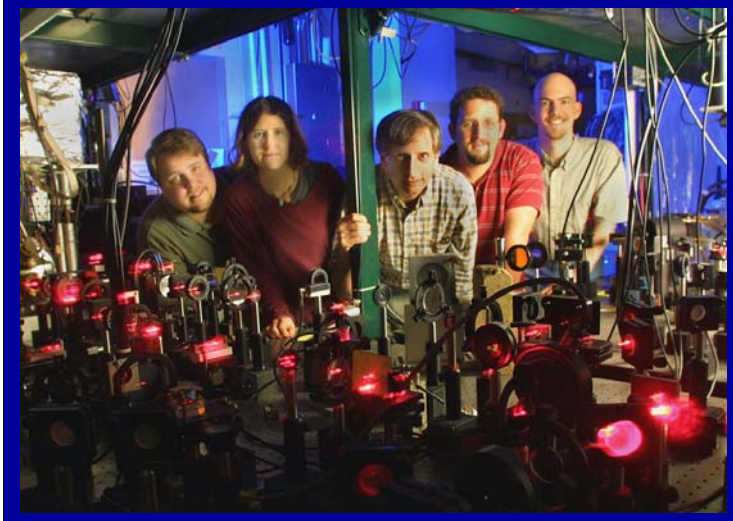

Mike Gehm
Staci Hemmer
John Thomas
Ken O'Hara
Stephen Granade

Joe Kinast
Andrey Turlapov

Fast Rotating Scalar and Multi-Component Bose Gases

Tin-Lun (Jason) Ho
Physics Dept, The Ohio State University

We show that in the limit of large angular momentum, many equilibrium and dynamical phenomena of scalar and multi-component Bose gases can be accounted for by approximating the system to reside in an effective lowest Landau level (1), (2), (3). This method explains the origin of the mysterious stripe formation in fast rotating Bose gas recently observed at JILA (4), and accounts for all the dynamical details observed in this experiment. To further demonstrate the usefulness of this method, we present its predictions of the interference patterns of two vortex lattices (5), and rich vortex lattice structures in multi-component Bose gases (6).

(1) Tin-Lun Ho, PRL 87, 060403 (2001).
(2) Erich Mueller and Tin-Lun Ho, PRL 88, 180403 (2002)
(3) Erich Mueller and Tin-Lun Ho, accepted for publication by PRA.
(4) P. Engels, I. Coddington, P. C. Haljan, and E. A. Cornell , PRL, 89, 100403 (2002)
(5) and (6): E. Mueller and T.L. Ho, to be published.

Microgravity Electron Electric Dipole Moment Experiment with a Cold Atom Beam

Harvey Gould

MS 71-259,
Lawrence Berkeley National Laboratory,
Berkeley, CA, 94720

INTRODUCTION

New physics beyond the Standard Model: The small CP violation contained in the Standard Model is insufficient to account for the baryon/antibaryon asymmetry in the universe [Sakharov; 1967]. New sources of CP violation are provided by extensions to the Standard Model. They contain CP-violating phases that couple directly to leptons and from which a large electron electric dipole moment (EDM) may be generated. Observation of an electron EDM would be proof of a Standard Model extension because the Standard Model only allows an electron EDM of less than 10^{-57} C-m (S.I. units; 1 C-m = 1.6 x 10^{-21} e-cm). A null result, however, constrains models and improving the limit tightens constraints, further restricting the models.

Any discovered new source of CP-violation not contained in the Standard Model will immediately lead to the question "How strongly does it couple to leptons?" The electron EDM experiment is the experiment that can best answer that question - better than any high energy physics experiment: the electron is stable and it can be precisely probed inside an atom. And the attractiveness of an electron EDM experiments using atoms is that it is sensitive only to a CP violating coupling to leptons - there is no existing effect to be subtracted out.

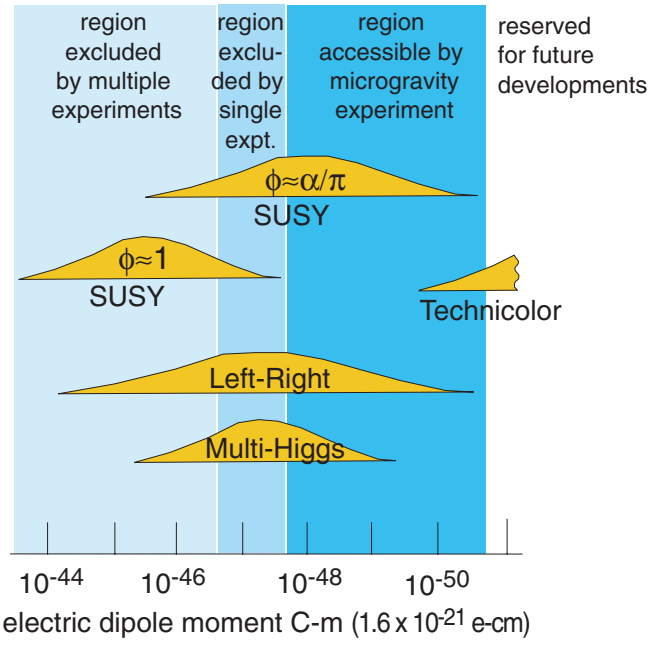

Fig.1: Electron EDM predictions and experimental upper limits in S.I. units (1 C-m = 1.6 x 10^{-21} e-cm) based upon Fig. 1 of [Pendlebury & Hinds, 2000]. The shape of the theory limit envelopes are not intended to represent any distribution of models.

A microgravity electron EDM experiment can achieve a greater sensitivity than a laboratory experiment because in microgravity the atoms travel slowly, at a uniform velocity, allowing a far greater interaction time, reducing the linewidth and better cancelling motional systematic effects.

Electron EDM experiments using atoms - Electron EDM experiments search for an EDM in a neutral atom (or molecule). The atom establishes a neutral sys-

tem and may provide an enhancement to the electron EDM. This enhancement, R, the ratio of an atomic EDM to a (valence) election EDM, is a relativistic effect and reaches large values for many high atomic-number atoms. It is 115 ±15 for the ground state of cesium [Johnson et al., 1986; Sandars; 1966]. Most important, the discovery of an electron EDM, far larger than predicted by the Standard Model, *does not depend upon the error in the calculated enhancement effect being small.*

Electron EDM experiments search for a change in a transition energy upon reversal of an external electric field. The electric field reversal separates a time-reversal (T) violating and parity (P) violating EDM from the T- and P- allowed quadratic Stark effect (Fig. 2). The experiment looks for a change in transition energy between different m_F levels (z projections of the total angular momentum $\mathbf{F} = \mathbf{I}+\mathbf{J}$ where I = 7/2 is the nuclear spin in Cs and J = 1/2 is the electronic angular momentum of the $6^2S_{1/2}$ state). Using both the F = 4, $m_F = -4 \rightarrow m_F = 3$ and F = 4, $m_F = 4 \rightarrow m_F = -3$ transitions to search for the EDM subtracts out the contribution of an incomplete reversal of the electric field and the first order effect of any residual magnetic field. Other transitions can be used to test for systematic effects. For example, the F = 4, $m_F = -4 \rightarrow m_F = 1$ transition is some thirty times more sensitive to motional systematic effects. This allows one to distinguish a true EDM from the most troublesome systematic effect. In the absence of an EDM or systematic effect, there is no observed effect.

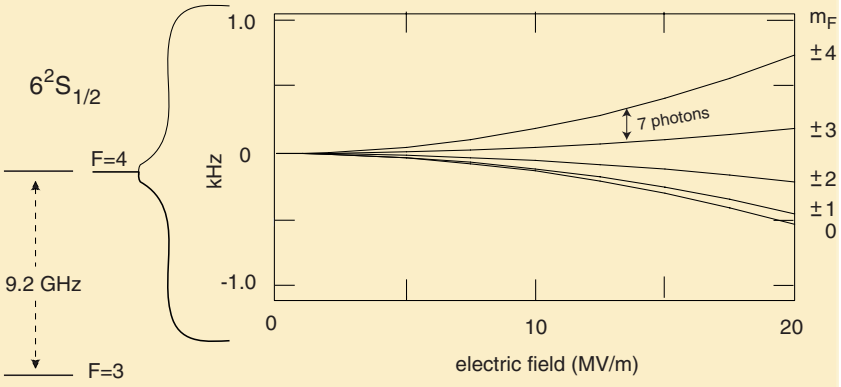

Fig. 2. Quadratic Stark effect in the cesium $6^2S_{1/2}$ F = 4 ground state. There is no magnetic field. The effect is quadratuc in E and therefore unchanged upon a reversal of E. An electron EDM however, adds a linear term that scales as E.

Since 1964 the majority of electron EDM experiments have used atomic beams in free space, unperturbed by light or frequent collisions; a feature shared by atomic clocks, which they resemble. Not surprisingly, the development of atomic beam EDM experiments has followed the development of atomic clocks and it is expected that EDM experiments will follow laser-cooled atomic clocks into microgravity.

EXPERIMENT

Experimental overview: The signature of the EDM is a net shift in the $m_F = 4 \rightarrow m_F = -3$ and $m_F = 3 \rightarrow m_F = -4$ transition frequencies upon reversal of the electric field. Cesium atoms launched from a megneto-optic trap at 0.1 m/s - 0.2 m/s (and cooled in the moving frame to 2 μK) enter a set of electric field plates with no voltage applied (Fig. 3). The voltage is then applied when the atoms are between the plates. This avoids acceleration of the atoms by electric

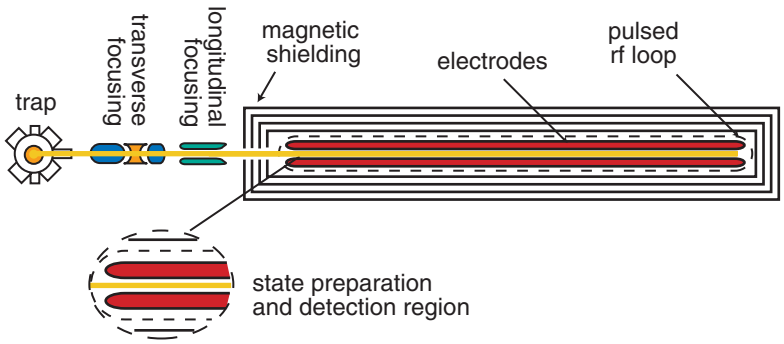

Fig. 3. Schematic of a slow atom microgravity electron EDM experiment

field gradients and defocusing effects from the fringe fields. After one second the field has stabilized and charging currents subsided. The $m_F = +4$, $F = 4$ level of the $6^2S_{1/2}$ state is populated by optically pumping and an oscillatory field, perpendicular to the electric field is applied. This oscillatory field induces a seven photon transition from the $m_F = 4$ level to the $m_F = -3$ level or from the $m_F = -4$ level, to the $m_F = 3$, level (Fig. 2). The experiment will switch between the two sets of initial and final states.

When, in microgravity, the atoms, traveling at 0.2 m/s though the electric field plates, reach the opposite end they will be reflected by the electric field gradient. At 0.2 m/s and in a field of 21 MV/m they will penetrate until the electric field drops by 0.14%. At this point their longitudinal velocity is zero, and they reverse direction and accelerate back to 0.2 m/s.

The reflection is identical for both electric field polarities and the brief 0.14% change in field will not affect the Ramsey resonance or the EDM measurement. As the atoms near the electric field plate entrance the oscillatory field is applied for the second time.

Atoms making the seven-photon transition to the $m_F = -3$ (or $m_F = 3$) of the $F = 4$ level will be optically pumped into the $F = 3$ hyperfine level of the $6^2S_{1/2}$ state. From here they are cycled to the $F = 2$ level of the $6^2P_{3/2}$ state and the fluorescence photons detected. The atoms remaining in the $m_F = 4$ (or $m_F = -4$) level are measure, for normalization, by detecting the fluorescence photons from the cycling transition to the $F = 5$ level of the $6^2P_{3/2}$ state.

Multiple quantum transitions and linewidth: The linewidth is determined by the interaction time (in this case about ten seconds) and the multiplicity of quanta in the transition. The linewidth will be further narrowed by using seven identical photons in the $m_F = 4 \rightarrow m_F = -3$ and $m_F = -4 \rightarrow m_F = +3$ transitions. If the photons are identical (and certain other conditions are met), the linewidth is shared among the 7 quanta and the observed linewidth is narrowed by roughly a factor of 7 [Gould et al., 1969; Gould, 1976; McColm, 1996].

Motional magnetic field effect: To be sensitive to an electron EDM, measurements will be made between levels of different $|m_F|$ which also makes the measurements sensitive to internal and external magnetic fields. The most infamous of these is the motional magnetic field effect.

The motional magnetic field, B_{mot} seen by a neutral atom moving through a static electric field E, with a velocity v, is given (S.I. units, lowest order) by $B_{mot} = vxE/c^2$ where v is the velocity of the atom, E, the electric field, and c, the speed of light. The magnitude of B_{mot} remains

constant upon a reversal of E. However when B_{mot} is added to an external magnetic field, B_0 a component of the magnetic field in the direction of E can change when E is reversed.

The interaction of the atom's *magnetic* dipole moment with this magnetic field component, which changes synchronously with the electric field reversal, mimics an EDM. An external magnetic field, B_0 has here to fore been used to lift the degeneracy between the m_F levels, allowing transitions between them. The elimination of this and other residual magnetic fields (such as those 1 nT fields remaining after magnetic shield deGaussing) will greatly reduce the motional magnetic field effects.

Electric field quantization: The systematic due to motional magnetic fields can be reduced far below experimental sensitivity by making the interaction with the electric field much larger than the interaction with the magnetic field (electric field quantization) [Player and Sanders; 1970.]

The J = 1/2 ground states in alkali atoms have very small electric field splittings between the $|m_F|$ levels (Fig. 2) and electric field quantization is feasibly only by eliminating all external magnetic fields. Even then, the electric field splittings are too small for resonance transitions in a thermal atomic beam experiments with transition linewidths of several hundred Hz . However the extremely narrow linewidth of a cold atom microgravity experiment makes it feasible to use electric field quantization in the alkali ground state.

ACKNOWLEDGMENTS

The work described here is being done in collaboration with Jason Amini. This work is supported by the Office of Biological and Physical Research, Physical Sciences Research Division, of the National Aeronautics and Space Administration. The Lawrence Berkeley National Laboratory is operated under U.S. Department of Energy Contract No. DE-AC03-76SF00098.

REFERENCES

Gould et al.; 1969: H. Gould, E. Lipworth, and M.C. Weisskopf, "Quadratic Stark Shift between Zeeman Substates in Cs^{133}, Rb^{87}, Rb^{85}, K^{39}, and Na^{23}," Phys. Rev. **188**, 24 (1969).

Gould; 1976: H. Gould, "Tensor polarizability of the ground-state hyperfine structure of thallium," Phys. Rev. A**14**, 922 (1976).

Johnson et al.; 1986: W.R. Johnson, D.S. Guo, M. Idrees, and J. Sapirstein, "Weak-interaction effects in heavy atomic systems. II," Phys. Rev. A**34** 1043 (1986).

McColm; 1996: D. McColm, "Ramsey patterns for multiquantum transitions in fountain experiments," Phys. Rev A**54**, 4842 (1996).

Pendlebury and Hinds; 2000: J.M. Pendlebury, and E.A. Hinds, "Particle electric dipole moments," Nucl. Instrm. Meth. A**440** 471 (2000), and references therein.

Player and Sandars; 1970: M.A. Player and P.G.H. Sandars, "An experiment to search for an electric dipole moment in the $^3P_2$ metastable state of xenon," J. Phys. B**3**, 1620 (1970).

Sakharov; 1967: A. D. Sakharov, ""CP violation and baryonic asymmetry of the Universe," ZhETF Pis. Red. **5** (1967) 32; JETP Lett. **5** (1967) 24.

Sandars; 1966: P.G.H. Sandars " Enhancement factor for the electric dipole moment of the valence electron in an alkali atom, " Phys. Lett. **22**, 290 (1966).

Evaporative cooling in a Holographic Atom Trap

Raymond Newell
University of Wisconsin- Madison

We present progress on evaporative cooling of ^{87}Rb atoms in our Holographic Atom Trap (HAT). The HAT is formed by the interference of five intersecting YAG laser beams: atoms are loaded from a vapor-cell MOT into the bright fringes of the interference pattern through the dipole force. The interference pattern is composed of Talbot fringes along the direction of propagation of the YAG beams, prior to evaporative cooling each Talbot fringe contains 300,000 atoms at 50 μK and peak densities of 2×10^{14} cm^{-3}. Evaporative cooling is achieved through adiabatically decreasing the intensity of the YAG laser. We present data and calculations covering a range of HAT geometries and cooling procedures.

RACE AND CALCULATIONS OF THREE DIMENSIONAL DISTRIBUTED CAVITY PHASE SHIFTS

Ruoxin Li and Kurt Gibble, The Pennsylvania State University,
State College, PA

1. ABSTRACT

The design for RACE, a Rb-clock flight experiment for the ISS, is described. The cold collision shift and multiple launching (*juggling*) have important implications for the design and the resulting clock accuracy and stability. We present and discuss the double clock design for RACE. This design reduces the noise contributions of the local oscillator and simplifies and enhances an accuracy evaluation of the clock.

As we try to push beyond the current accuracies of clocks, new systematic errors become important. The best fountain clocks are using cylindrical TE_{011} microwave cavities. We recently pointed out that many atoms pass through a node of the standing wave microwave field in these cavities. Previous studies have shown potentially large frequency shifts for atoms passing through nodes in a TE_{013} cavity. The shift occurs because there is a small traveling wave component due to the absorption of the copper cavity walls. The small traveling wave component leads to position dependent phase shifts. To study these effects, we perform Finite Element calculations. Three-dimensional Finite Element calculations require significant computer resources. Here we show that the cylindrical boundary condition can be Fourier decomposed to a short series of two-dimensional problems. This dramatically reduces the time and memory required and we obtain (3D) phase distributions for a variety of cavities. With these results, we will be able to analyze this frequency shift in fountain and future space clocks.

2. INTRODUCTION

The principal advantage of microgravity for atomic clocks is interrogation times longer than 1 s. With a 10 s interrogation time, a clock has a 50 mHz linewidth suggesting that accuracies may approach 10^{-17}. However, to achieve greater accuracy within the same averaging time, greater stability is needed. RACE is based on Rb to avoid the large cold collision shift of Cs.[1,2] This may allow simultaneously high short-term stability and accuracy. We have three primary goals: (1) Demonstrate new clock techniques for laser-cooled atoms to enable frequency comparisons with accuracies of 1 part in 10^{17}. (2) Significantly improve the classic clock tests of general relativity. (3) Distribute accurate time and frequency from the ISS. We review the design constraints and discuss the double clock design for RACE.

Current atomic fountain clocks have inaccuracies near 10^{-15}. Losses in the microwave cavities lead to small traveling wave components that deliver the power from the cavity feed to the walls of the cavity.[3] The small traveling wave components produce a microradian distribution of phases throughout the cavities, and therefore distributed cavity phase shifts need to be considered. LeMonde *et al.* have shown that there are large phase shifts in multi-Rabi TE_{013} cavities due to the traveling wave

component near the nodes of the standing wave.[4] These phase shifts produce large frequency shifts of order 10^{-13} for $\pi/2$ excitation and 10^{-11} for $3\pi/2$ pulses.

Using finite element analysis to study the TE_{011} microwave cavity, we found that there are nodes through which the atoms pass.[5] The nodes occur in the cut-off waveguide sections used to prevent microwave leakage from the cavity. By symmetry, the lowest coupled mode is the TE_{01}. The longitudinal magnetic field in the TE_{01} waveguide mode reverses between the center and the copper boundary. Therefore, there must be a node in the time-dependent field the atoms experience as they pass through the cavity with trajectories near the waveguide wall. Hence one might expect large phase shifts due to traveling wave components for these atoms.

Three-dimensional Finite Element calculations require significant computer resources. Here we show that the boundary condition on the cylindrical cavity walls can be Fourier decomposed in a basis of $\cos(n\varphi)$.[6] This reduces the 3D problem to a Fourier series of 2D problems. Because the atoms pass through the center of the cavity and because the wave equation solutions are proportional to ρ^n, only 3 to 4 terms in the series are required to accurately calculate the 3D phase of the microwave field. This reduces hours of calculations to seconds. With these results, we can analyze the frequency shifts in earth and space clocks due to distributed cavity frequency shifts.

3. DESIGN OF JUGGLING CLOCKS AND RACE

To achieve the potential accuracy of laser-cooled microgravity clocks with reasonable integration times, atoms must be multiply launched (juggled). Juggling imposes several constraints on the design of a microgravity clock. Shutters are needed to block the light scattered from trapping, state preparation, and detection from the interrogation region. In Figure 1, we show a design for a juggling

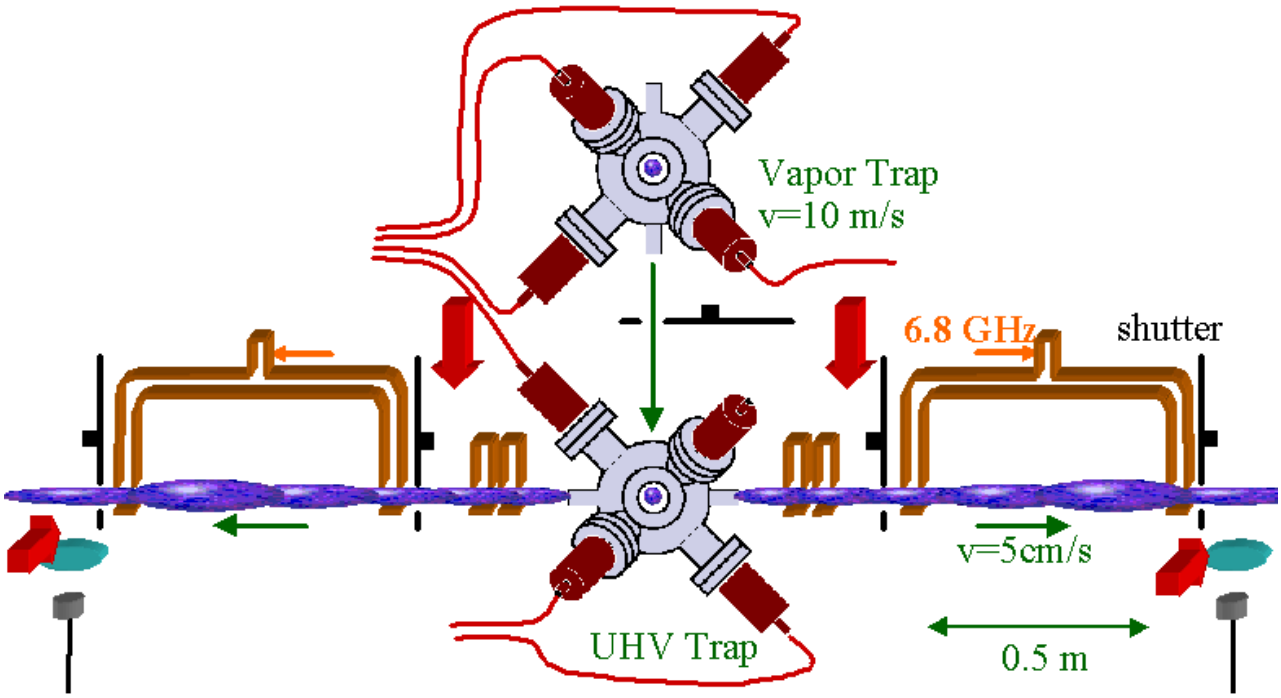

Figure 1. Schematic for juggling microgravity Rb clock RACE. The double MOT launches atoms at high speed from the (upper) vapor trap to the (lower) UHV trap so that the shutter between the traps can be nearly always closed. The shutters between the UHV trap and the cavities are nearly always open except during the ≈5ms that the light for the UHV trap is turned on. The atoms are alternately launched left or right to go through one clock cavity or the other.

microgravity clock that has a pair of shutters surrounding the Ramsey cavity. This is a design for our Rb microgravity clock, RACE. First we discuss the laser trapping and cooling techniques and then the advantages of having 2 clock cavities.

The double-MOT[7,8] allows a high throughput of cold atoms and therefore a high short-term stability. The high throughput is possible because the double-MOT can rapidly capture many cold atoms and then efficiently launch them through the Ramsey cavity. The "upper" vapor cell trap in Fig. 1 essentially continuously traps atoms and then launches them at 5-10 m/s to the UHV trap "below." Because of the high launch velocity from the vapor cell trap, the atoms pass quickly through the shutter separating the 2 traps. This implies that the shutter only needs to open for the short time that the ball of atoms flies through, and only during that time must the lasers for the vapor-cell trap be extinguished to prevent light from entering the interrogation region.

The real advantage of the double-MOT design comes from the fact that the UHV trap can capture and launch a ball of atoms in as little as 5 ms. This implies that the shutter separating the UHV trap and interrogation region only has to close for 5 ms for each launch and therefore is nearly always open. This allows a high throughput since, if the shutter is ~10 cm from the center of the UHV trap, the ball of atoms will have expanded considerably before reaching the shutter. For our juggling Cs experiment,[8] it was crucial to reduce the trapping and cooling time of the UHV trap be able to study collisions at low energies (corresponding to juggling rates as high as 140 s^{-1}.

One also has to worry about the effect of the trapping light on the previously launched ball of atoms from the 2nd trap. Again, this was a crucial step in our Cs juggling experiment. By "hiding" the ball in the lower hyperfine state immediately after the launch, and by carefully controlling the low intensity repumping light to the 2nd trap, we can capture and launch balls of atoms almost on top of one another.[8]

The RACE schematic in Fig. 1 shows 2 clock cavities. After atoms are collected in the lower laser trap, they are launched either through one cavity or the other. Having 2 cavities is important for a number of reasons. One advantage is that it greatly reduces the requirements for the local oscillator. Few oscillators can perform at the $\sigma_y(\tau) = 3\times10^{-15}\ \tau^{-½}$ level and there would be significant work required to develop their flight worthiness. The essential problem with only a single cavity results from the fact that the microwave frequency fed to the cavity must be changed from one side of the transition to the other. During the switch-over, all of the atoms must be cleared from the cavity and this means the oscillator is not tracked for about 10 s when T = 10 s. With 2 cavities, we can do the switch-over for one cavity while still monitoring the oscillator with the other cavity and therefore the stability of the clock is so affected by the local oscillator instability.

Vibrations on the ISS in the direction of the launch velocity cause a noise in the interrogation time. With 2 cavities, the 2 detected signals will behave oppositely so that the effects of vibrations can be identified, correlated with an accelerometer, and removed. Furthermore, one of the largest systematic errors is the AC Stark shift due to blackbody radiation at 300K. A measurement of the red shift and time dilation with frequency inaccuracies of 10^{-17} demands absolute knowledge of the average temperature in the clock cavity at the 0.01K level. Having 2 cavities will allow a critical check on our accuracy evaluation. In addition, having 2 cavities gives important redundancy. For example, if a shutter fails in the closed position, we will still be able to achieve mission success goals (although requiring longer averaging times).

4. CALCULATIONS OF DISTRIBUTED CAVITY PHASE SHIFTS

Nearly all current primary fountain clocks use a cylindrical TE_{011} cavity to excite the atoms. In Figure 2, we show contours of the magnitude of the longitudinal magnetic field (H_z) in a TE_{011} cavity. Those atoms that pass near the wall of the waveguide when they enter or exit the cavity first experience a field that is reversed (π phase shift) relative to that at the center of the cavity.[5] Therefore, there must be nodes for atoms passing near the walls and, from [4], one could expect large phase errors for atoms passing through these regions. In fact, atoms going through nearly half of the area of the aperture on each pass see a field reversal and therefore a node in the field.

Losses in the cavities imply there is a small traveling wave component in addition to the large standing wave. The traveling wave component leads to phase gradients in the cavity.[3,9] Therefore, atoms passing through different regions, especially different regions on the upward versus downward passages, see a different effective phase of the microwave field. This can lead to a frequency shift of the clock known as the distributed cavity phase shift.[10] The distributed cavity phase shifts can be particularly large at nodes of the field as the traveling wave dominates at the nodes of the standing wave.

The traveling wave field, due to the losses, is not easy to calculate analytically – it mixes many modes. Khursheed, Vecchi, and DeMarchi used a finite element method to calculate the traveling wave field and the phase shifts for an infinitely long two-dimensional cylindrical cavity.[9] Extending the calculations to three dimensions requires vastly greater memory and computation time; the time required scales as $T_{2D}^{3/2}$. Here we show that the three dimensional problem can be expressed as a quickly converging series of two-dimensional problems. This shortens calculations requiring hours on current personal computers to seconds.

Following Khursheed, Vecchi, and DeMarchi, we can decompose the microwave field in the cavity into a standing wave H and a small traveling wave g.[9] Here, we are particularly interested in the z components (along the cylindrical axis) of these fields. H, g, and, by superposition, H+g are solutions to Maxwell's equations. The boundary conditions for H_z are zero on the top and bottom endcaps and a zero normal derivative on the cylindrical walls of the cavity and the cut-off waveguide sections. For g_z, the boundary conditions on the top and bottom endcaps is $g_z = \frac{1+i}{\sqrt{2\sigma\mu\omega}} \nabla\times\left(\hat{n}\times H\right)\hat{z}$ and the normal derivative on the cylindrical walls is $\frac{\partial g_z}{\partial n} = (1-i)\sqrt{\frac{\omega\varepsilon_0}{2\sigma}} k\, H_z$ where $\omega = 2\pi\times 9.192$ GHz, ε_0 is the vacuum permittivity, μ is the vacuum permeability, σ is the conductivity (of copper), and k is the microwave wave vector. These cavities are

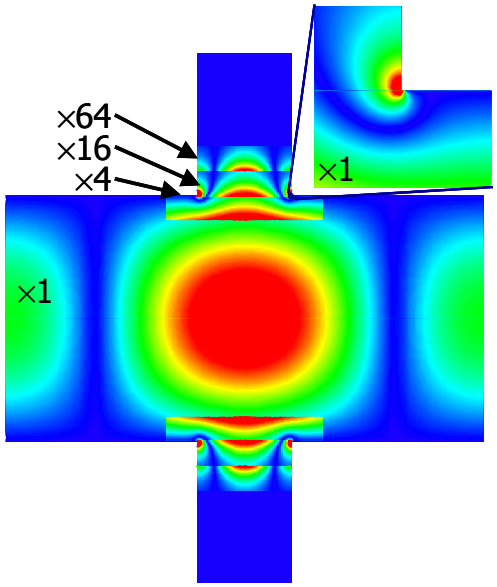

Figure 2. Contours of the magnitude of the longitudinal magnetic field, H_z, in a cylindrical TE_{011} cavity. The cavity height 26.075 mm, the radius is 25.5 mm, and the apertures have a 1cm diameter. The field near and in the cut-off waveguide sections are magnified by 4, 16, and 64 times. The line of field nodes (blue) in the below cut-off waveguide sections extend into the cavity and can be clearly seen in the magnified section. The field strength, where the cut-off section meets the cavity (red), is comparable to the peak field in the (red) center of the cavity (with π phase shift).

fed by one, two, or four small holes distributed around the cavity's midsection. At the feed, the boundary condition for $\partial g_z/\partial n$ is given by balancing the power fed into the cavity against the losses in the walls. An example of the boundary condition at the midsection for a single cavity feed is shown in Figure 3.

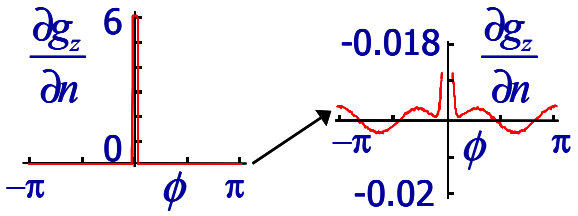

Figure 3. Boundary condition for the traveling wave field g_z at the midsection of a cavity with a single feed. Power is supplied at $\varphi \approx 0$ and there are small losses at all other φ. The 1% variation of the losses is due to the proximity of the TE_{311} modes and could be neglected.

The boundary condition in Figure 3 can be expressed as a Fourier series $\sum_n A_n(z)\cos(n\phi)$ and we can write $g_z(\rho,\phi,z)=\sum_n g_n(\rho,z)\cos(n\phi)$.[6] Then, g_n satisfies the two-dimensional wave equation

$$\left[\frac{1}{\rho}\frac{\partial}{\partial\rho}\left(\rho\frac{\partial}{\partial\rho}\right)-\frac{n^2}{\rho^2}+\frac{\partial^2}{\partial z^2}+k^2\right]g_n(\rho,z)=0 \quad (1).$$

Because the feed is very small, to preserve a cavity Q > 10,000, many n are required to get the full solution of g_z; as the feed approaches a delta function, $n \to \infty$ is required. However, for $\rho \to 0$, the

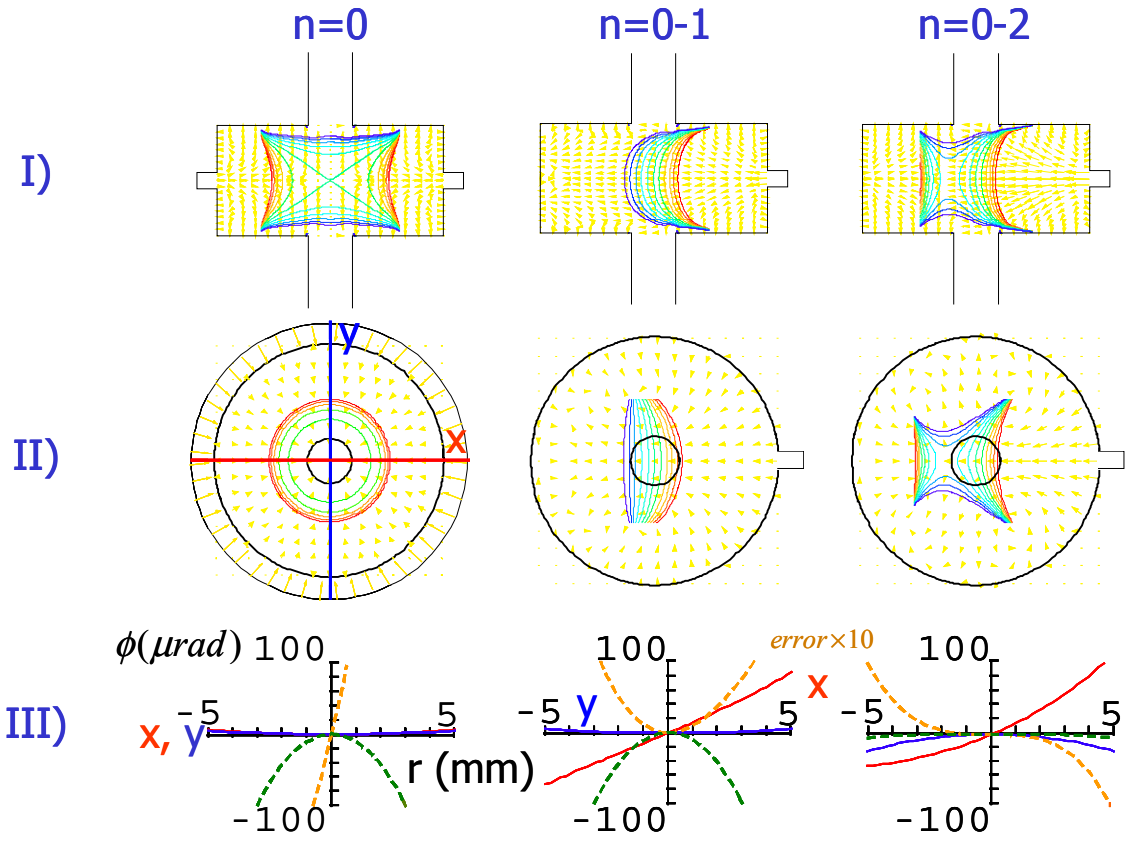

Figure 4a. Phase contours of H_z+g_z and the Poynting vector in I) the x-z plane and II) the z=0 plane. Phase contours are 25 µrad steps. Each is shown for 1,2, & 3 terms in the azimuthal expansion. III) The phase (solid line) and errors (dashed lines) plotted versus x and y for z=0. The error is the difference between the phase for N terms versus that for 65 terms. For 3 terms (n=0-2), the maximum phase error in the central region is ≈10%.

asymptotic solution to Eq. 1 is ρ^n. Since the atoms pass through the center of the cavity, g_n, for large n, has a negligible effect and, as we show next, only $n \leq 2$-3 is required.

We Solve Eq. 1 on a triangular lattice for the cavity in Figure 2 for a variety of cavity feeds. For a single cavity feed, we choose the feed to be on the positive x-axis. The solution is symmetric about the x-y plane. (The solution is also symmetric about the x-z plane and therefore g_z is an expansion in $\cos(n\varphi)$.) We therefore mesh $\rho, z \geq 0$ with 3,200 to 50,000 triangles and solve for g_n with n=0-64.[11]

In Figures 4a and 4b, we show the phase contours and Poynting vectors from a sum of g_n for n=0-N for N=0-4 & 64. The n=0 term exactly describes a cavity that is fed azimuthally symmetrically at the midsection. Therefore, this term has very small phase gradients and the Poynting vectors show power flowing in at the midsection and flowing to all the other surfaces. For the n=1 midsection, power is supplied for positive x and, for negative x, power is removed to nearly balance that supplied by n=0. Higher n further distributes the power in the plane to construct the small feed. Due to the proximity of the TE_{311} resonance, the n=3 term has a noticeable effect on the power flow in the cavity. The series converges very rapidly; for 3 terms, the phase error near the center of the cavity is ≈10% and for 4 terms it is less than 1%. The rapid convergence shows that the atoms are insensitive to localized cavity losses at surfaces far from the atoms' trajectories – it is only the average absorbed power over $\Delta\varphi \approx \pi/4$ that affects the phase of the microwave field seen by the atoms. Irregularities in the cut-off waveguide sections, especially where the field is large near the junction of the cut-off section and the cavity, may have important effects.

Cavities with two and four feeds are commonly used.[12] These avoid the large flow of power across a cavity with a single feed that leads to the large phase gradient along the x axis shown in Figs. 4. In Fig. 5, we show calculations for two and four feeds. For two (four) feeds, g_z is a sum over g_n for

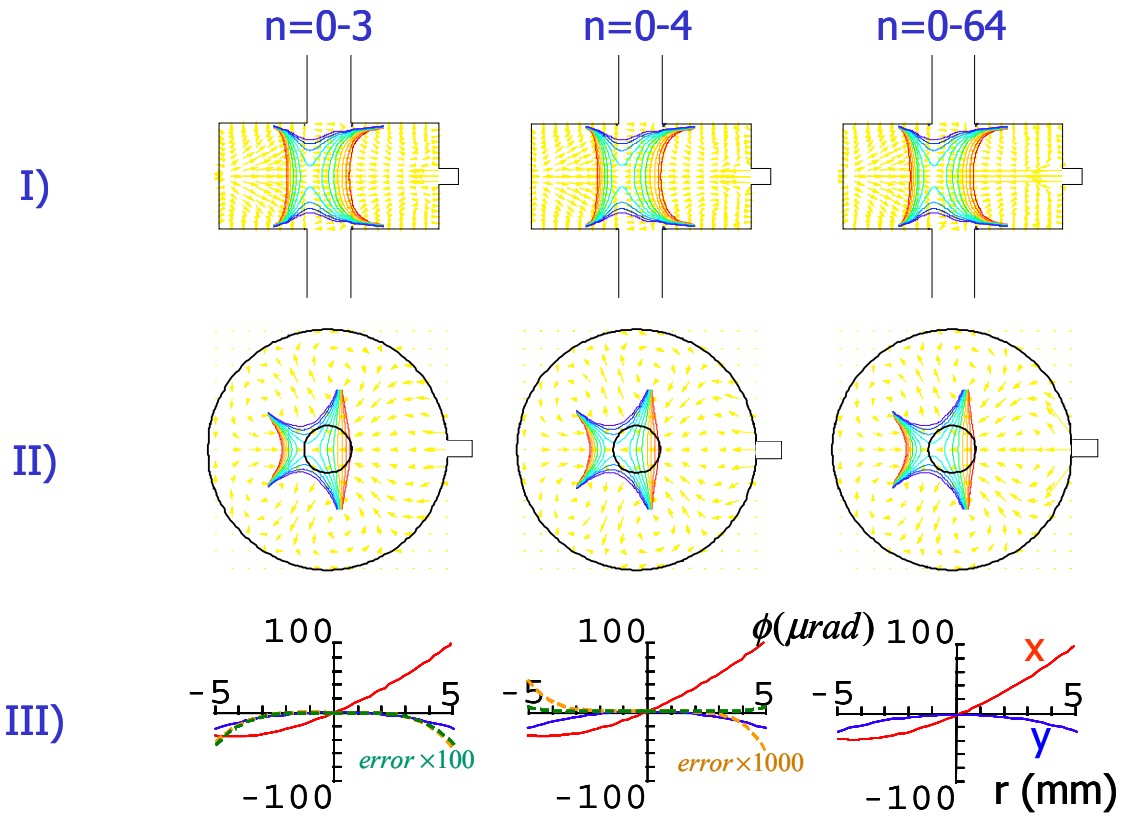

Figure 4b. The same quantities in Fig. 4a for 4, 5, and 65 terms of the azimuthal expansion. For 4 terms, the error is less than 1% or 1μrad.

n=0,2,4,6, … (0,4,8,12,…). These show significantly smaller phase gradients than a cavity with a single feed.

Armed with the three dimensional phase in the cavity, the atomic responses to the microwave field can be calculated. The dramatically faster computation of a series of 2D calculations will facilitate the optimization of cavities for atomic clocks. We are currently analyzing the effects of the large phase shifts near the standing wave nodes. This is important for the currently operating atomic clocks. For future clocks, it is not difficult to eliminate the nodes. One cavity design that eliminates this potential error is shown in Figure 6.[5] A larger diameter section of cut-off waveguide is used. In this large diameter section the nodes are not sampled by the atoms and the field decays to a sufficiently small level. Then the smaller diameter waveguide section, which sets the cavity aperture, follows to insure a sufficiently small microwave leakage.

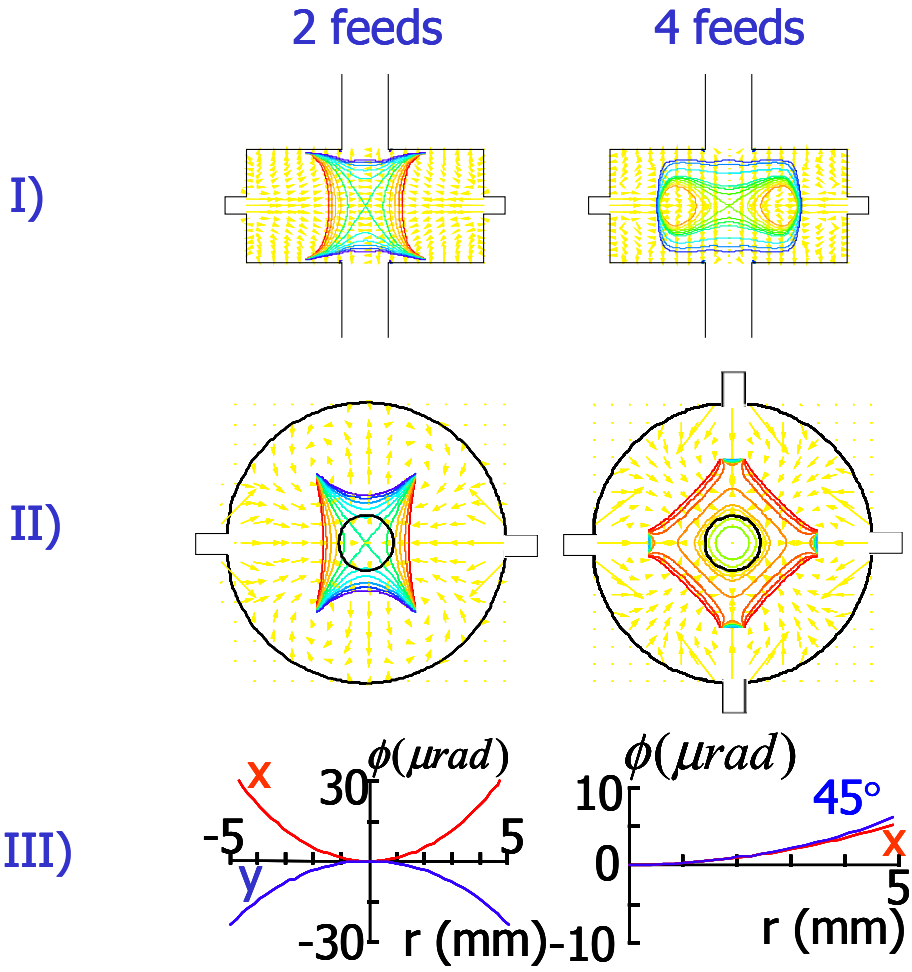

Figure 5. Phase contours of H_z+g_z and the Poynting vector for cavities fed by 2 and 4 ports in I) the x-z plane and II) the z=0 plane. Phase contours are 25 μrad steps. III) The phase for z=0 plotted versus x and y for the 2 feeds and versus x and along x=y for 4 feeds. Both show smaller phase gradients than a cavity with a single feed.

5. CONCLUSIONS

To achieve the potential accuracy of laser-cooled microgravity clocks with reasonable integration times, atoms must be multiply launched (juggled). The short-term stability is proportional to the launch rate and this in turn implies that high accuracy and stability favor long interrogation regions. Laser-cooled microgravity clocks can achieve short-term stabilities approaching $\sigma_y(\tau) = 3\times10^{-15}\ \tau^{-½}$. At this stability, the largest uncertainty in a Cs microgravity clock is likely to be the cold collision frequency shift. By using ^{87}Rb, the collision shift is 50 times smaller allowing an accuracy of 10^{-17}. We describe the design of our Rb microgravity clock which uses a double-MOT and 2 cavities. This simplifies the trapping and shutter design while maintaining a high throughput of cold atoms, minimizes

the local oscillator requirements, eliminates errors due to vibrations, and provides failure and accuracy redundancy.

The commonly used TE_{011} cylindrical cavities have nodes in the field regions sampled by the atoms. Near the nodes there may be significant phase shifts, especially near the wall of the cutoff waveguide apertures, and this effect may interact with other errors to produce a tilt sensitivity of fountain clocks.

We have shown that the 3D distribution of the phase of the microwave field in a cavity can be expressed as a 2D azimuthal expansion. This dramatically reduces the needed computing time (and memory). These gains will facilitate improvements in microwave cavity designs for earth and space-based atomic clocks.

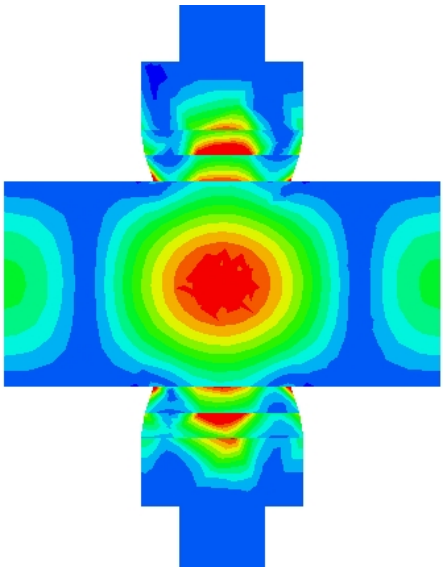

Figure 6. Contours of the magnitude of H_z in a cylindrical TE_{011} cavity with cutoff waveguide sections of different diameter. The larger diameter waveguide sections have nodal lines outside of the region through which atoms pass. In the smaller diameter section, H_z, while it has nodes, can be sufficiently small.

6. ACKNOWLEDGEMENTS

We acknowledge financial support from the NASA Microgravity program and Penn State University.

7. REFERENCES

[1] C. Fertig and K. Gibble, Phys. Rev. Lett. **85**, 1622 (2000).
[2] K. Gibble and S. Chu, Phys. Rev. Lett. **70**, 1771 (1993).
[3] G. Vecchi and A. De Marchi, IEEE Trans. Instr. Meas. **42**, 434 (1993).
[4] P. Lemonde, G. Santarelli, Ph. Laurent, F. Pereira, A. Clairon, and Ch. Salomon, Proceeding of the Freq. Contr. Symp., p. 110, (1998)
[5] C. Fertig, R. Li, J. I. Rees, and K. Gibble, Proc. 2002 IEEE Freq. Contr. Symp., 469 (2002).
[6] C.L. Britt, IEEE Trans. Antenna and Propagat. **37**, 1181 (1989) ; Y. Chen, R. Mittra, P. Harms, IEEE Trans. Microwave Theory and Tech. **44**, 832 (1996).
[7] K. Gibble, S. Chang, and R. Legere, Phys. Rev. Lett. **75**, 2666 (1995).
[8] R. Legere and K. Gibble, Phys. Rev. Lett. **81**, 5780 (1998).
[9] Khursheed, Vecchi, & DeMarchi, IEEE Tran. UFFC **43**, 201, 1996.
[10] A. Bauch, T. Heindorff, and R. Schroeder, IEEE Trans. Instrum. Meas. 34, 136 (1985).
[11] For n=0, the wave equation has a scaler solution for g_z that does not satisfy Maxwell's equations. For n=0, we solve instead for the $\hat{\varphi}$ component of the electric field and obtain the magnetic field from it.
[12] See for example A. Clairon, S. Ghezli, G. Santarelli, Ph. Laurent, S. N. Lea, M. Bahoura, E. Simon, S. Weyers, and K. Szymaniec, Proc. Fifth Symp. Freq. Standard and Metrol., 49 (1995); C. R Ekstrom, E.A. Burt, T.B. Swanson, Proc. 2001 IEEE Freq. Contr. Symp., 53 (2001); S.R. Jefferts, R.E. Drullinger, A. DeMarchi, Proc. 1998 IEEE Freq. Contr. Symp., 6 (1998); S. Weyers, U. Hubner, R. Schroder, C. Tamm, A. Bauch, Digest 2000 Conf. Prec. Electromagnetic Meas., 632 (2000); F. Levi, L. Lorini, D. Calonico, A. Godone, IEEE Trans. Instr. Meas., **52**, 267 (2003).